Received: 2 July 2024 | Accepted: 12 February 2025

DOI: 10.1111/jpy.70006

RESEARCH ARTICLE

A comparison of calcification mechanisms in haploid and diploid cells of the coccolithophore *Calcidiscus leptoporus* (Murray & Blackman 1898)

Erin M. Meyer | **Alison R. Taylor**

Department of Biology and Marine Biology, University of North Carolina Wilmington, Wilmington, North Carolina, USA

Correspondence
Alison R. Taylor, Department of Biology and Marine Biology, University of North Carolina Wilmington, Wilmington, NC 28403, USA.
Email: taylora@uncw.edu

Funding information
Division of Ocean Sciences, Grant/Award Number: 1638838; Division of Biological Infrastructure, Grant/Award Number: 1229024 and 1828053

Editor: N. Poulsen

Abstract

Coccolithophores are prominent marine pelagic calcifiers due to their production of calcite coccoliths. Diploid coccolithophores produce heterococcoliths intracellularly, with an organic cellulose baseplate scale acting as a nucleating substrate. However, coccolith production in the haploid life phase has not been extensively studied. Most haploid coccolithophores produce distinct holococcoliths that were previously thought to be produced in an extracellular space. However, we recently observed intracellular holococcolith production in haploid *Coccolithus braarudii*. We therefore compared the calcification mechanisms of the 2N and N phases of *Calcidiscus leptoporus*, an understudied yet ecologically important species, to better understand ultrastructure features related to calcification and explore aspects of the calcification pathway in each life-history phase. We show that both life phases of *C. leptoporus* produce coccoliths intracellularly and that holococcoliths are likely nucleating on body scales in a dilated vacuole space rather than within a tightly associated coccolith vesicle (CV) as in diploid heterococcolith production. Both life phases were sensitive to the SERCA Ca^{2+}ATPase inhibitor thapsigargin, suggesting conservation in the transcellular Ca^{2+} transport pathways utilized for intracellular calcification, namely through calcium accumulation in the endoplasmic reticulum. However, the Si analogue germanium led to severe disruption of the CV and coccolith morphogenesis only in the diploid life phase. This work provides strong evidence to support a model of intracellular holococcolith production and clearly demonstrates that calcification in both life phases shares a common cellular pathway. Nevertheless, differences in the spatial arrangement of the CV membrane exert significant control over crystal growth that has profound consequences for coccolith morphology.

KEYWORDS
biomineralization, calcification, calcium transport, coccolithophore, haploid, Heterococcolith, holococcolith, silicon, ultrastructure

Abbreviations: ANOVA, analysis of variance; CAP, coccolith-associated polysaccharides; CV, coccolith vesicle; DMSO, Dimethyl sulfoxide; EDS, energy dispersive spectroscopy; ER, Endoplasmic reticulum; HET, heterococcolith-bearing cell (typically diploid); HOL, holococcolith-bearing cell (typically haploid); PIC, particulate inorganic carbon; POC, particulate organic carbon; SEM, scanning electron microscopy; SERCA, Sarco/Endoplasmic Reticulum Ca^{2+}-ATPase; TEM, transmission electron microscopy.

INTRODUCTION

The life history of coccolithophores is characterized by calcified haploid (N) and diploid (2N) life stages (Green et al., 1996; Klaveness & Paasche, 1971; Vargas et al., 2007). In natural environments, the 2N phase is typically dominant (Young et al., 2003) while the N phase arises in response to a variety of environmental cues through meiotic cell division to produce motile cells. In a few cases, haploid cells are uncalcified, as seen in *Emiliania huxleyi* (Klaveness & Paasche, 1971), a species now referred to as *Gephyrocapsa huxleyi* after recent phylogenetic analysis (Bendif et al., 2023). In both life stages, populations are maintained through asexual reproduction.

The factors that determine coccolithophore life-phase transitions have been examined in both laboratory-based culture studies and field observations (Frada et al., 2009; Noel et al., 2004). The presence of cells bearing a combination of both hetero- and holococcoliths has been documented for a wide range of coccolithophores isolated from field samples (Geisen et al., 2002; Young et al., 2005). In laboratory studies, it has been demonstrated that the non-calcifying (naked) phenotype of *Gephyrocapsa huxleyi* can be promoted in response to viral infection (Frada et al., 2008), with or without a change in ploidy (Frada et al., 2017), which corresponds to increased resistance to infection (Mordecai et al., 2017). Life-phase transitions in response to a variety of culture manipulations have also been documented (Houdan et al., 2006; Laguna et al., 2001; Noel et al., 2004), which has led to the hypothesis that high light, stable, and nutrient-limited oligotrophic waters induce transition to the N stage, while turbulent and nutrient-replete conditions typical of coastal waters favor the 2N stage (Houdan et al., 2006). The haplo-diplontic life cycle of coccolithophores expands the niche space they can occupy (Vries et al., 2021) and is an evolutionary strategy that could allow for their survival in a rapidly changing ocean (D'Amario et al., 2017; Vargas et al., 2007). Moreover, a switch to predominantly N life stage populations, with a lower particular inorganic carbon:particulate organic carbon (PIC/POC ratio), may significantly reduce net calcification rates and carbon export from the surface oceans (Daniels et al., 2016; Iglesias-Rodriguez et al., 2002).

The 2N life stage of coccolithophores is typically characterized by the presence of heterococcoliths (HET). These calcite structures are produced in an intracellular Golgi-derived vesicle known as the coccolith vesicle (CV). A specialized organic scale within the CV promotes nucleation of a protococcolith ring by acting as a substrate for nucleating molecules, such as CAP or ion complexes bringing Ca^{2+} and CO_3^{2-} to the site of nucleation (Marzec et al., 2019; Young, 1989). The protococcolith ring comprises repeating V (sub-vertical) and R (sub-radial) calcite crystal units that undergo anisotropic growth to form a range of species-specific morphologies (Avrahami et al., 2022; Young et al., 1992, 1999). The CV membrane is tightly associated with the growing heterococcolith crystal surfaces (Drescher et al., 2012; Taylor et al., 2007), and the cytoskeleton is thought to play an important role in morphogenesis (Kadan et al., 2021; Langer et al., 2010). The type and morphology of coccoliths are species-specific. For example, 2N *Scyphosphaera apsteinii* has two types of coccoliths—a flat murolith and a barrel-like lopadolith (Drescher et al., 2012)—while 2N *Coccolithus braarudii* produces interlocking placoliths of the same type (Taylor et al., 2007; Young, 1987). The N stage of coccolithophores appears to always be motile and typically produces holococcoliths that are much smaller and composed of an organic scale covered with minute isotropic rhomboidal calcite crystals, implying that the mechanism of calcification significantly differs between life stages (Noel et al., 2004; Young et al., 1999). This is supported by studies that demonstrate differing sensitivities to calcification disrupters. When grown in the presence of the Si transport inhibitor germanium (Ge), calcification is disrupted in some Si-requiring heterococcolith-bearing species (Durak et al., 2016); however, the holococcolith-bearing phases of these same species do not show Ge sensitivity or a Si requirement for normal calcification (Langer et al., 2021). This suggests mechanistic differences in HOL coccolith formation, but the mode of calcification for holococcolith-bearing cells remains poorly understood.

Rowson et al. (1986) proposed that holococcoliths are produced extracellularly based on the absence of observable internal calcified structures (Klaveness, 1973; Manton & Leedale, 1963a, 1963b) and because of a thin layer, or "skin," covering the calcite layer, which could allow for calcification in an extracellular space. Work by Cros et al. (2013) supported this proposed mechanism based on observations of relatively high magnesium (Mg) associated with holococcolith calcite compared to low-Mg calcite of heterococcoliths, suggesting their formation was extracellular. However, recent work has provided evidence for internal holococcolith calcification. Across various species, both Langer et al. (2021) and Ben-Joseph et al. (2023) observed calcite rhombs associated with organic scales in internal vesicles using transmission electron microscopy (TEM). Furthermore, scanning electron microscopy (SEM) and X-ray dispersive spectroscopy determined no detectable Mg in holococcoliths, implying the presence of low-Mg calcite consistent with cation fractionation expected for intracellular, rather than extracellular, calcification (Langer et al., 2021).

Even with internal holococcolith calcification, the cellular mechanisms involved must differ from heterococcolith production. Langer et al. (2021) proposed that heterococcoliths may have evolved after

holococcoliths with the advent of additional cellular machinery, such as coccolith-associated polysaccharides (CAP), that can lead to more control over crystal growth and intricate morphologies, whereas holococcoliths are produced by inorganic crystal nucleation and isotropic growth. Therefore, other structural elements related to calcification, such as the reticular body, could be absent in the holococcolith-bearing phase. Additionally, the organic scale used for coccolithogenesis differs between holo- and heterococcolithogenesis. It has been well established that an organic, cellulose baseplate scale provides nucleating sites for heterococcoliths and can vary widely in size, thickness, and arrangement of microfibrillar material (Billard & Inouye, 2004; Marsh, 1999; Taylor et al., 2007; Westbroek et al., 1989; Young et al., 1999). The baseplate scale is thought to influence aspects of the final coccolith, such as the overall size, which may be correlated to the final coccolith mass through the inclusion of more protocrystals during nucleation (Beuvier et al., 2019; Young, 1989). A recent multispecies analysis of baseplate scales using high-resolution cryo-EM imaging concluded that the CV chemical environment, in addition to the species-specific surface properties of the organic scale, exerts tight control over nucleation patterns and subsequent morphological crystal growth (Eyal et al., 2022). Coccolithophores also possess unmineralized body scales, a characteristic trait of the haptophytes, which are also produced in the Golgi and secreted onto the cell surface between the plasma membrane and the coccosphere (Billard & Inouye, 2004). As with baseplate scales, there is a variety of body scale morphologies, with some evidence that the type of body scale may be associated with specific life phases (Houdan et al., 2004).

Regarding the evolution of coccolithogenesis, Langer et al. (2021) recently speculated that the last common ancestor of the Calcihaptophycidae gained the ability to mineralize a body scale, comprising clusters of small rhombohedral crystals (i.e., holococcoliths). Coccolithophores subsequently evolved more regulatory machinery (e.g., modified organic scales, polysaccharides, and protein complexes) that enabled the production of more morphologically complex heterococcoliths. Additionally, as with heterococcoliths, holococcolith size seems to correlate with body scale size (Braarud et al., 1955), implying that holococcolith body scales could perform a similar function to HET baseplate scales. Ultimately, further study on holococcolith-associated organic scales is warranted as this can not only increase our knowledge of the mechanisms of holococcolith production but can also provide insight into how calcification evolved in the coccolithophores (Langer et al., 2021).

To further understand the mechanistic differences between holococcolith and heterococcolith production, we performed ultrastructural and morphological studies of diploid heterococcolith-bearing (HET) and haploid holococcolith-bearing (HOL) *Calcidiscus leptoporus* cells. *Calcidiscus leptoporus* is an understudied, yet environmentally important coccolithophore that is cosmopolitan, and regionally, it can produce significant calcite, such as in the South Atlantic (Baumann et al., 2004). Its large heterococcoliths preserve well in sediments and, with one of the longest fossil records, have been used extensively as paleoproxies, helping elucidate past sea surface temperatures, salinity, and productivity (Renaud & Klaas, 2001; Silva et al., 2009; Stoll et al., 2002). It is important that we understand *C. leptoporus* calcification mechanisms in order to robustly develop them as paleoproxies and also to better predict how calcite production by this species, and therefore local PIC export, may be impacted by a changing climate. Despite their importance, no comprehensive ultrastructural study of *C. leptoporus* has been published to date, leaving gaps in our understanding of its calcification mechanisms.

Our results represent a detailed ultrastructure analysis of both life phases of *Calcidiscus leptoporus*, an ecologically important coccolithophorid that provides new insights into coccolithogenesis and robust evidence supporting a model of intracellular holococcolith production in a relatively unconstrained space (Ben-Joseph et al., 2023; Langer et al., 2021).

METHODS

Maintenance of algal cultures

Both 2N and N *Calcidiscus leptoporus* (RCC 1130) from the Roscoff Culture Collection were grown in 40-mL batch cultures of autoclaved and filter-sterilized Gulf Stream seawater. Haploid *C. leptoporus* arose spontaneously as a result of leaving diploid cultures undisturbed at ~75 μmol photons · m^{-2} · s^{-1} light for 3–6 weeks. Once the presence of motile calcified N cells was visually confirmed, cells were drawn from the top of an undisturbed culture and further batch cultured to ensure no diploid cells were carried over. The diploid phase of *C. leptoporus* was grown in seawater supplemented with LH nutrients and vitamins (Fowler et al., 2015), and N *C. leptoporus* was grown in LH/8. All cultures were maintained at 15°C on a 14:10 h light:dark cycle, at approximately 100 μmol photons · m^{-2} · s^{-1}.

Haploid and diploid *Calcidiscus leptoporus* sensitivity to Ge

Calcidiscus leptoporus HET and HOL cells were grown in 2 μM Si LH media and in media supplemented with various Ge concentrations. Media for Si-limitation experiments was prepared with no added Si, and Si

concentration was measured prior to adding sufficient $NaSiO_3$ to reach the necessary 2 μM Si. [Si] was measured with a Bran+Luebbe Autoanalyzer (AA3, Bran+Luebbe GmbH, Germany) using the molybdate method, combining oxalic acid, ascorbic acid, and molybdate reagents that were modified from Brzezinski and Nelson (1995) and Brzezinski et al. (1997). Prior to each analytical run, the reagent lines were flushed with 0.6% sodium dodecyl sulfate (SDS) to lubricate them and ensure consistent flow of samples. Saturated oxalic acid ($143\,g \cdot L^{-1}$) was used to overcome any phosphate interference. Molybdate was made fresh for each run. Germanium was added in the form of GeO_2 to reach the following Si:Ge ratios: 1:1, 1:2.5, and 1:10 (2 μM Si : 2 μM Ge, 2 μM Si : 5 μM Ge, and 2 μM Si : 20 μM Ge, respectively). A control group was included where no Ge was added. Replicate ($n = 4$) 40-mL cultures were seeded with washed cells for a starting density of ~$1 \times 10^4\,mL^{-1}$ and maintained at the same temperature and light conditions as described previously. Cells were grown for 10 d, and aliquots for estimating growth rates were collected every other day. Aliquots for SEM were taken at mid- and late-exponential stages (i.e. 6 and 10 days).

Cell counting

Cells were counted using a hemocytometer or Sedgwick-Rafter chamber. A minimum of 300 cells was counted per replicate flask. Growth curves were plotted, and maximum growth rates (exponential phase) were calculated for each species by calculating the slope of the growth curve typically between day 2 and day 6 using the following equation:

$$\text{Rate of increase } (r) = \frac{\left(\ln\left(C_{t_2}\right) - \ln\left(C_{t_1}\right)\right)}{\left(t_2 - t_1\right)}$$

Where C is the average cell number per L at time t, t_1 is the start day, and t_2 is the end day of the range of days used to calculate maximum r.

Scanning electron microscopy

For SEM observations, 1–3 mL of culture were gently syringe-filtered onto 13 mm, 0.4 μm isopore filters (Merck Millipore Ltd.) and followed by a further 4 mL MilliQ water buffered with 1 mM HEPES (pH 8.0) to remove seawater salts while preventing the dissolution of coccolith calcite. Filters were air-dried and mounted onto an SEM stub with carbon adhesive tabs before coating with 10 nm Pt/Pd or Au/Pd. Samples were imaged using a FEI Apreo FEG-SEM (FEI/Thermo Scientific, Hillsboro, Oregon) in standard imaging mode using an external secondary electron (Everhart-Thornley) detector at a working distance of 7–7.5 mm with a primary beam acceleration of 5 keV and spot size 3. In some cases, a lower incident beam energy and shorter working distance were used to visualize fine-scale structures such as base plate scales with predominantly backscattered electrons using the T1 detector.

Effects of Ge on *Calcidiscus leptoporus* ultrastructure

For Ge disruption experiments, four replicates of *Calcidiscus leptoporus* HET and HOL were grown in LH or LH/8 with a [Si] of ~100 μmol. Diploid heterococcolith-bearing *C. leptoporus* calcification is disrupted at a 1:0.2 Si:Ge ratio; therefore, cells were exposed to 100:20 μM Si:Ge to ensure disrupted calcification without cell death. The cultures were monitored with light microscopy to assess when calcification had been sufficiently disrupted to sample and prepare for TEM analysis.

Transmission electron microscopy processing and image collection

For TEM ultrastructural analysis, 3-mL aliquots of cells were harvested and fixed with 1:1 mixture of 5% glutaraldehyde and HEPES-buffered seawater (pH = 8.6) for 1 h, then centrifuged for 10 min at 10,000 rpm (8500 *g*). The pellet was resuspended in 0.2 M sodium cacodylate buffer three times, with centrifugation as needed. The pellet was then secondarily fixed with 1% osmium tetroxide in 0.2 M sodium cacodylate buffer for 1 h and washed twice. An ethanol (EtOH) dehydration series followed (50, 75, 95, 2 × 100% EtOH), with EtOH mixes made with 50 mM calcium chloride nanopure water to prevent the dissolution of coccolith calcite during processing. The pellet was next imbedded in Spurr's epoxy resin and cured at 70°C for at least 8 h. Sections were cut using a diamond knife and Reichert-Jung (Leica) Ultra-cut E Microtome to thicknesses of 90–100 nm. Sections were collected on formvar-coated 200 mesh copper grids and stained with Reynolds lead citrate (Reynolds, 1963; buffered to pH 10.7 with 1 M NaOH) for 15 min. Grids were loaded into a Thermo Technai BioTWIN TEM and sections imaged using 80 KeV beam acceleration. Images were acquired with an Eagle 2000 K digital camera at 2048 × 2048 pixel resolution.

En bloc imaging of *Calcidiscus leptoporus* HOL

Resin embedded cells prepared for TEM were also imaged using SEM to further analyze populations of

cells for the presence of intracellular holococcoliths. Transmission electron microscopy resin blocks were faced with an ultramicrotome and then trimmed to a size that could be mounted stably on an aluminum SEM stub. These resin blocks were carbon coated (10 nm) and imaged using the FEI Apreo FEG-SEM with a beam acceleration of 5 keV and using the T1 detector with a working distance of 3.5–4 mm, which resulted in images primarily comprising backscattered electrons.

Negative staining

Three-milliliter aliquots of calcifying and non-calcifying haploid *Calcidiscus leptoporus* were harvested and fixed with a 1:1 mixture of 5% glutaraldehyde:HEPES-buffered seawater at a pH of 8.6 (final glutaraldehyde v/v = 2.5%) for 1 h, then centrifuged at 10,000 rpm (8500 *g*) for 10 min. The pellet was washed with a 0.2 M sodium cacodylate buffer (pH = 8.6) three times, then fixed for 1 h with 1% osmium tetroxide made in 0.2 M sodium cacodylate buffer, followed by three washes with the sodium cacodylate buffer. The cells were stored at 4°C until used, at which point the pellet was gently resuspended. One drop of cells was pipetted onto a formvar coated Cu grid, and cells were allowed to settle. Any excess liquid was gently removed with blotting paper. For haploid cells, one drop of Reynold's lead citrate (adjusted to pH 10.7) was then placed on the grid for 1–3 min, with the removal of excess liquid with blotting paper. Diploid phase cells were stained with 2% uranyl acetate for 30 min.

Investigation of Ca^{2+} transport pathway

Batches of *Calcidiscus leptoporus* HET and HOL were grown in the presence of the Sarco/Endoplasmic Reticulum Ca^{2+}-ATPase (SERCA) blocker thapsigargin (Enzo Biosciences catalogue # BML-PE180-000 or AdipoGen catalogue # AG-CN2-0003-M001) to investigate whether they both utilize an endoplasmic reticulum (ER) Ca^{2+} transport pathway to the coccolith vesicle (CV). A 10-mM thapsigargin stock solution was prepared in anhydrous dimethyl sulfoxide (DMSO) and 30-mL replicates ($n = 4$) of cells were grown in each of the following conditions: a media control, a DMSO control, and two thapsigargin concentrations (0.5–5.0 μM) selected to be sublethal for both HET and HOL cells. The resulting DMSO control concentrations were 0.025% and 0.05% vol/vol for the HET and HOL experiments, respectively. After 24 and 48 h, cells were counted, and *F*v/*F*m measurements were taken using an AquaPen AP 100 fluorometer (PSI, Drasov, Czech Republic). At 48 h, 0.5–2-mL aliquots were collected for SEM analysis.

Growth of the cultures was assessed by the change in cell number between 24 and 48 h. Coccolith morphology was scored based on different criteria for HET and HOL and is indicated in the respective figures. Coccoliths were only scored if the majority of the coccolith could be seen. A minimum of 60 cells and 340 heterococcoliths were scored for each replicate. Scores for each morphometric category are presented as the average of the experimental replicates ($n = 4$).

Statistics

*F*v/*F*m, cell counts, and coccolith morphology were statistically analyzed through a series of one-way analyses of variance (ANOVAs). A Shapiro-Wilk test for normality was run, and if the data passed, Brown-Forsythe and Holm-Sidak tests were performed to compare differences between the experimental groups and control samples. If the data were not normally distributed, then a Kruskal-Wallis and Dunn's test was performed to assess differences between groups.

RESULTS AND DISCUSSION

Diploid *Calcidiscus leptoporus* produced round calcite heterococcoliths that interlocke between proximal and distal shields to form a coccosphere that encloses the cell (Figure 1). Motile haploid *C. leptoporus* cells possessed two flagella and a single short haptonema appendage between them (Figure 1a). The haploid cell lay within the calcified layer of holococcoliths with a significant space between the cell and the holococcosphere (Figure 1a,b). Holococcoliths of *C. leptoporus* were comprised of two rows of stacked calcite rhombs, with a third layer around the periphery of the holococcolith (Figure 1c).

Ultrastructure of *Calcidiscus leptoporus* HET

Transmission electron microscopy analysis demonstrated that *Calcidiscus leptoporus* HET shares very similar ultrastructural features to coccolithophore species that produce large placolith-type heterococcoliths, such as *Coccolithus braarudii* (Taylor et al., 2007, Figure 2). Two chloroplasts were arranged at the periphery of the cell surrounding the nucleus and associated cytoplasm. A prominent Golgi complex with characteristic dilated and thickened cisternae was responsible for the production and secretion of body scales and was the origin of the CV. The CV was closely associated with the growing calcite coccolith (Figure 2a), which occupied a significant volume of the cell. Although a range of ER and vesicles was commonly associated with the developing CV, a morphologically distinct reticular

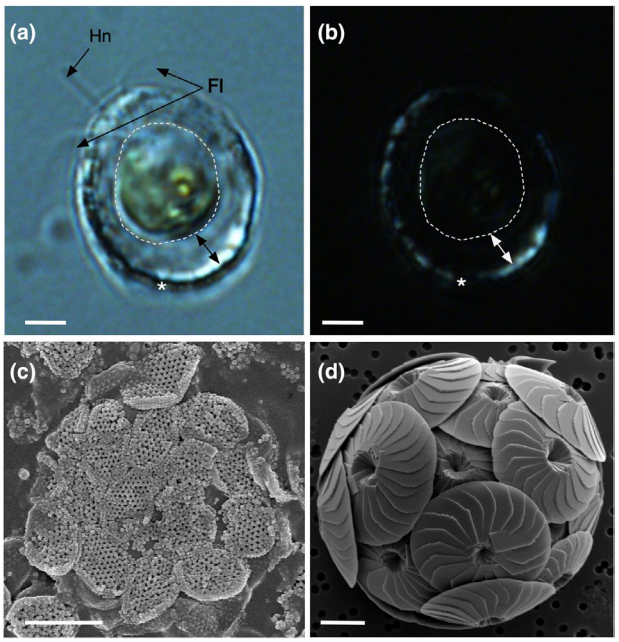

FIGURE 1 Haploid and diploid *Calcidiscus leptoporus* features. (a) Differential interference contrast image of a haploid cell (white dotted line) within the surrounding holococcosphere (white asterisk). The single haptonema (Hn) and pair of flagella (Fl) are indicated. The double headed arrow indicates the space that lies between the cell and the holococcosphere. (b) A polarized light image of the same cell in (a) emphasizing the calcite of the holococcosphere, position of cell, and space between them (white double headed arrow). (c) SEM micrographs of a HOL cell and (d) HET cell. Scale bars represent 2 μm.

body previously described in several HET species (Drescher et al., 2012; Taylor et al., 2007) was not observed in over 40 cell sections of *C. leptoporus* HET. However, a zone of vesicle exchange with the plasma membrane was frequently observed. In many cases, clusters of vesicles (~50 nm diameter) were observed just beneath the plasma membrane in the apical region of the cell, and some of these membrane invaginations were seen fused with the plasma membrane (Figure S1). Although this TEM data could not distinguish exocytosis from endocytosis, it is possible that the size and quantity of vesicles in these regions represented a zone of dynamic membrane retrieval after the coccolith was secreted. Fusion of the coccolith vesicle with the plasma membrane, allowing expulsion of the completed coccolith, has the potential to add a significant quantity of functionally distinct endo membrane to the cell plasma membrane. For example, a cell of 10 μm in diameter will have an approximate surface area of 314 μm^2, and the minimum vesicle membrane area for a 5-μm diameter coccolith would be ~30 μm^2, assuming a simple CV membrane morphology associated with the mature coccolith. This estimate suggests that every coccolith secreted has the potential to increase the cell surface area by ~10%, clearly not a sustainable process without efficient retrieval and recycling of the CV membrane. The observation of significant zones of large vesicles fused with or lying just below the plasma membrane

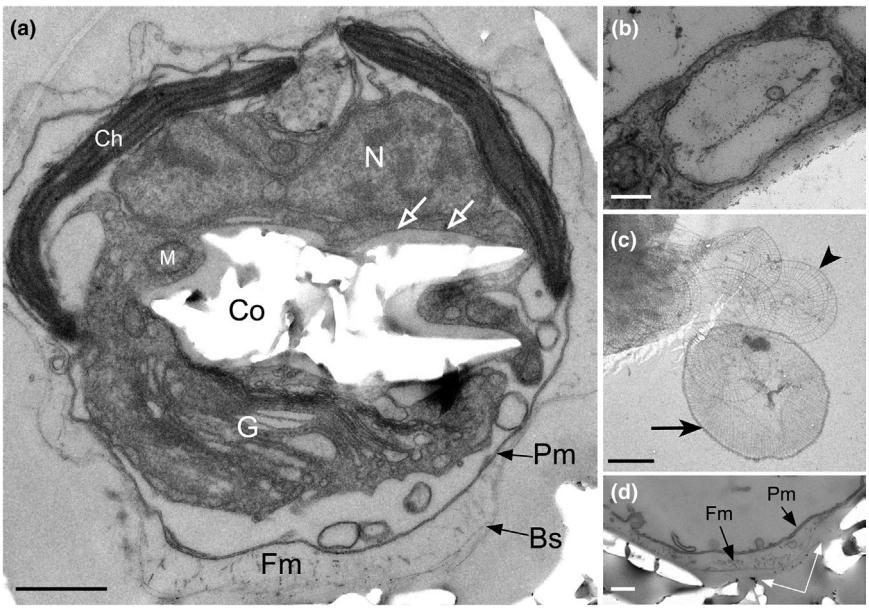

FIGURE 2 Ultrastructure of *Calcidiscus leptoporus* HET. TEM micrographs of cellular features (a) whole cell image. Bs, body scales; Ch, chloroplast; Co, heterococcolith; Fm, fibrillar material; G, Golgi; M, mitochondria; N, nucleus; Pm, plasma membrane; White arrows, coccolith vesicle membrane. (b) Body scale production in a loosely associated vesicle (c) Organic scales. Black arrow, baseplate scale; Black arrowhead, body scale. (d) Fibrillar material anchoring heterococcoliths to cell membrane. Fm, fibrillar material; Pm, plasma membrane; white arrows, organic baseplate scale. Scale bars represent; (a) 1 μm, (b) 200 nm, (c, d) 500 nm.

in *C. leptoporus* implies a recycling process and highlights the need for further detailed investigation. Once released onto the cell surface, heterococcoliths are integrated through interlocking distal and proximal shields into the coccosphere (see Figure 1d, Figure S1c). The extracellular space of the HET cell comprised fibrillar material that promoted close attachment of unmineralized body scales to the plasma membrane, which underlay the layer of interlocking mineralized coccoliths (Figure 2d).

A characteristic trait of the haptophytes is the presence of organic unmineralized body scales that are secreted to cover the cell. The arrangement of microfibers that comprise these scales can vary by species and life history phase (Eikrem et al., 2016). Diploid coccolithophores typically produce dimorphic organic scales that are produced intracellularly: the small body scales and the larger baseplate scales, the latter acting as a substrate for nucleating molecules during heterococcolith production. We conducted negative TEM staining of whole mount decalcified *Calcidiscus leptoporus* HET cells to determine the morphology of organic scales associated with these cells. Two distinct morphologies were observed: smaller rimless "lacey" body scales (length = 0.960 μm ± 0.101, $n = 9$, Table S1) with a loose arrangement of proximal surface radial and distal surface circular fibers and a larger (1.62 μm) more densely structured baseplate scale with a peripheral thickening and well-ordered proximal radial fibrils arranged in quadrants (Figure 2c, Table S1). The structure of the proximal and distal sides of the body scales in *C. leptoporus* HET was similar to the body scales observed in *Coccolithus pelagicus* HET, although in *C. leptoporus* the fibers appeared to be less densely packed (Houdan et al., 2004). The thickened rim of the baseplate scales was similar to those observed in other species, such as *Coccolithus pelagicus*, *Gephyrocapsa huxleyi*, and *Pleurochrysis carterae* (Eyal et al., 2022; Houdan et al., 2004; Marzec et al., 2019). Further SEM examination of the proximal surface of heterococcoliths confirmed the baseplate scale association with the central region of the coccolith and confirmed the mineralized baseplate (length = 1.582 μm ± 0.169, $n = 9$) was distinct from the smaller body scales (length = 0.956 μm ± 0.009, $n = 4$; Figure 3, Table S1). The dimorphism between *C. leptoporus* HET body scales and coccolith baseplate scales was consistent with observations from other HET species such as *Coccolithus pelagicus* (Houdan et al., 2004; Manton & Leedale, 1969). The *C. leptoporus* HET baseplate scales have a very similar structure and fiber arrangement to the HOL scales (Please refer to section titled: "Baseplate scales for holococcolith production are structurally similar to HOL body scales").

The HET baseplate scale presumably possesses some functionally critical properties that promote orderly nucleation and crystal growth in the CV. In a recent study using cryo-electron microscopy and 3D-Structured Illumination Microscopy (3D-SIM), Marzec et al. (2019) concluded that calcite nucleation on baseplate scales from *Pleurochrysis carterae* was dependent on positively charged primary amine functionalities that existed along the periphery of the baseplate scale. The positively charged rim of isolated baseplates attracted negatively charged poly (acrylic acid)-Ca^{2+} complex and poly(allylamine hydrochloride)-carbonate complexes to the

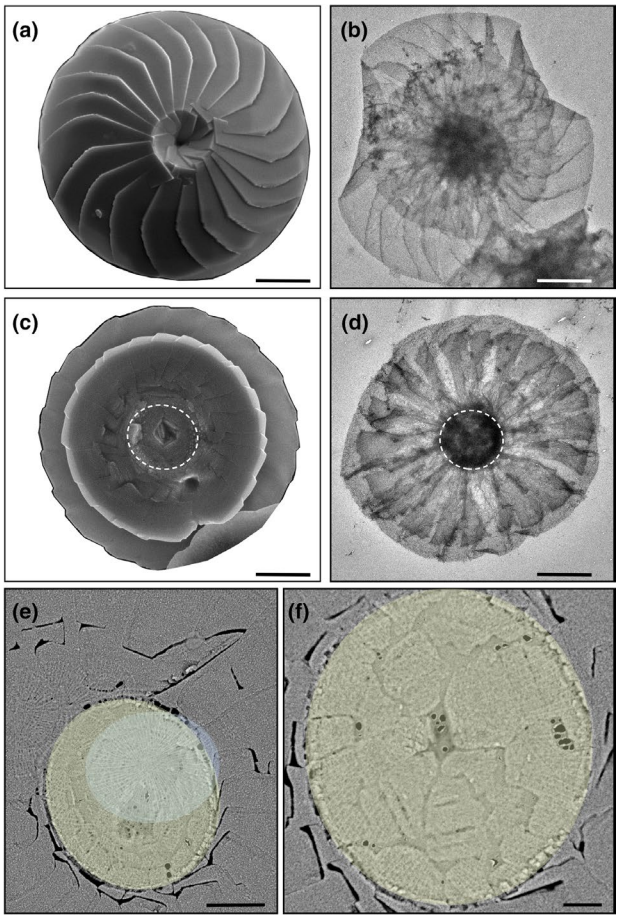

FIGURE 3 Organic phases associated with heterococcoliths of *Calcidiscus leptoporus*. (a) SEM micrograph of distal surface. (b) Negative stain TEM micrograph of distal view of residual organic material that remains after decalcification of heterococcoliths. The organic material associated with the proximal shield overlies the smaller diameter whorl of organic material associated with proximal shield. (c) SEM micrograph showing proximal view of coccolith. Central region associated with the baseplate scale is indicated with white dotted line. (d) Negative stain TEM micrograph of the proximal view of a decalcified heterococcolith showing the whorls of organics associated with the distal shield crystals that overlie the whorl of organics associated with the proximal shield. (e) Backscattered electron SEM image of proximal side of the heterococcolith showing the central region with coccolith baseplate scale (highlighted pale yellow) and a smaller bodyscale (highlighted pale blue). (f) Detail of a central proximal region showing the larger baseplate scale (highlighted pale yellow) with radial fibrils. Scale bars: (a–d) 1 μm, (e) 500 nm, (f) 200 nm.

rim of the distal side of the baseplate scale (Marzec et al., 2019). These complexes mimicked CAP-ion complexes theorized to transport Ca^{2+} and HCO_3^- to the baseplate scale. It has recently been argued that this model of HET baseplate nucleation may not be universal for HET cells (Eyal et al., 2022). Although in vitro mineralization experiments on isolated *P. carterae* baseplate scales confirmed a peripheral ring of Ca-rich dense phase, this was not observed for HET baseplate scales isolated from several other coccolithophore species (Eyal et al., 2022). Just as different CAP may play varying roles in influencing mineralization, it is possible that the differences in fiber arrangement observed among *Calcidiscus leptoporus, Gephyrocapsa huxleyi*, and *P. carterae* HET baseplate scales (Eyal et al., 2022) could underlie variations in how they mineralize.

Aside from the baseplate scale, the organic phases (surface and possibly intracrystalline) associated with each heterococcolith crystal were evident as organic material left after decalcification of heterococcoliths in the whole mount negative stained samples (Figure 3). This supports a role for CAPS in the control of anisotropic growth of the calcite units and highlights the need to better understand the functional roles of these organics. It is also important to recognize the incorporation and association of these organic phases into the coccolith (inorganic) fraction when estimating cycling and export of PIC/POC in surface oceans. Although the role of these organics has been implicated in the regulation of coccolith growth, morphogenesis, and the resistance of dissolution (reviewed in Walker & Langer, 2021), there is a lack of empirical information on the extent of coccolith-associated POC. For *Gephyrocapsa huxleyi*, it has been estimated that polysaccharides comprise 2.6 wt % of the coccoliths (Andersson et al., 2014) and direct measurements in bleached *G. huxleyi* coccoliths, in which surface organics are oxidized, reveal POC is 1.7 wt % (Subhas et al., 2018). For heavy calcifying species such as *Calcidiscus leptoporus* and *Coccolithus braarudii*, the POC associated with coccoliths (e.g., Figure 3b,d) may be significant yet remains an uncharacterized contribution to POC export that is inextricably linked to coccolith PIC export.

Ultrastructure of *Calcidiscus leptoporus* HOL and intracellular calcification

Transmission electron microscopy analysis of *Calcidiscus leptoporus* HOL allowed for a detailed description of the overall cellular organization that was consistent with the findings of other ultrastructure studies on haploid coccolithophores (Figure 4, Figure S2; Houdan et al., 2004, Parke & Adams, 1960). The cell with characteristic chloroplasts, mitochondria, and a prominent Golgi body constantly producing body scales (Figure S3) was surrounded by the calcified holococcosphere that

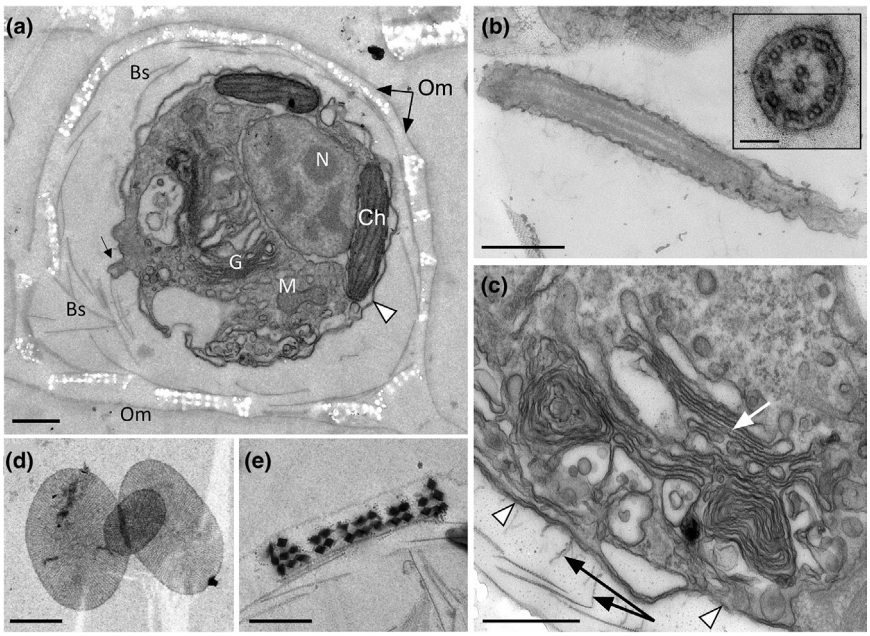

FIGURE 4 Ultrastructure of *Calcidiscus leptoporus* HOL. TEM micrographs of cellular features (a) Whole cell cross section Black arrow, flagellar root; Bs, body scales; Ch, chloroplast; G, Golgi; M, mitochondria; N, nucleus; Om, outer layer of amorphous organic material; Om, outer organic layer overlying the holococcosphere; White arrowhead, plasma membrane (b) Longitudinal section of a flagella with (inset) cross section of a flagella. (c) Golgi body producing scales. Black arrow, fibrillar material; White arrow, body scale; White arrow head, plasma membrane (d) Negative stain TEM of organic body scales. (e) Detail cross section of a holococcolith showing the arrangement and orientation of calcite rhombs on the organic scale. Scale bars represent (a) 1 μm, (b) 500 nm with inset = 100 nm, (c–e) 500 nm.

was covered by an outer amorphous organic layer (Figure 4a,e). A significant extracellular space separated the cell from the holococcosphere (Figure 4a, Figure 1), and an abundance of small body scales (Figure 4d) underlay the holococcosphere with scales more closely attached to the cell via fibrillar material associated with the plasma membrane (Figure 4c). The motile HOL cells exhibited two flagella and a haptonema (Figures 1 and 4b), and half (53%) of HOL cells analyzed displayed a large vacuolated space at the flagellar pole. These were the only major ultrastructural difference observed that could not be explained by expected life phase differences (Figure S4). Such vacuoles could help promote nutrient storage or optimal buoyancy, or be associated with phagotropy in these actively mixotrophic cells (Avrahami & Frada, 2020).

Clear evidence of intracellular calcification was observed in *Calcidiscus leptoporous* HOL cells by using the modified TEM sample preparation protocol that preserves calcite. In some cells, clusters of crystals were observed without any obvious associated scale, and it is possible this signifies disorganized extracellular calcified material that could be taken up into the cytoplasm through phagotrophy of these actively mixotrophic cells. However, numerous observations of cells were made in which an organic scale within a vesicle had one or more crystals associated with its surface (Figure 5a,b). In these cases, the vesicle was trans-Golgi, and the membrane was loosely associated with the mineralized scales, similarly to body scale production in HET (Figure 2b) cells.

En bloc imaging of *Calcidiscus leptoporus* HOL cells allowed for screening of many more cells than TEM sections and led to the discovery of fully calcified holococcoliths in a dilated intracellular vesicle and, in one case, multiple complete holococcoliths in a single vesicle (Figure 5c,d), presumably just prior to secretion. Holococcolith nucleation and maturation take place in a Golgi-derived vesicle (essentially a CV), are then secreted, and seem to initially adhere to the plasma membrane through fibrillar material. At some point, the holococcolith detaches from the cell membrane, traverses the extracellular space (Figure 5d, see also Figure 8c,d) and is incorporated into the holococcosphere. These observations in *C. leptoporus* supported recent results for *Coccolithus braarudii* and *Calyptrosphaera sphaeroidea* (Ben-Joseph et al., 2023; Langer et al., 2021). In all cases, the holococcolith crystals were observed in a dilated Golgi-derived vesicle. This is in marked contrast to heterococcoliths in which the CV membranes were in close association with the developing calcite structures throughout their development and supports results from Ben-Joseph et al. (2023) who observed holococcolith crystals in dilated vesicles within *Coccolithus braarudii*

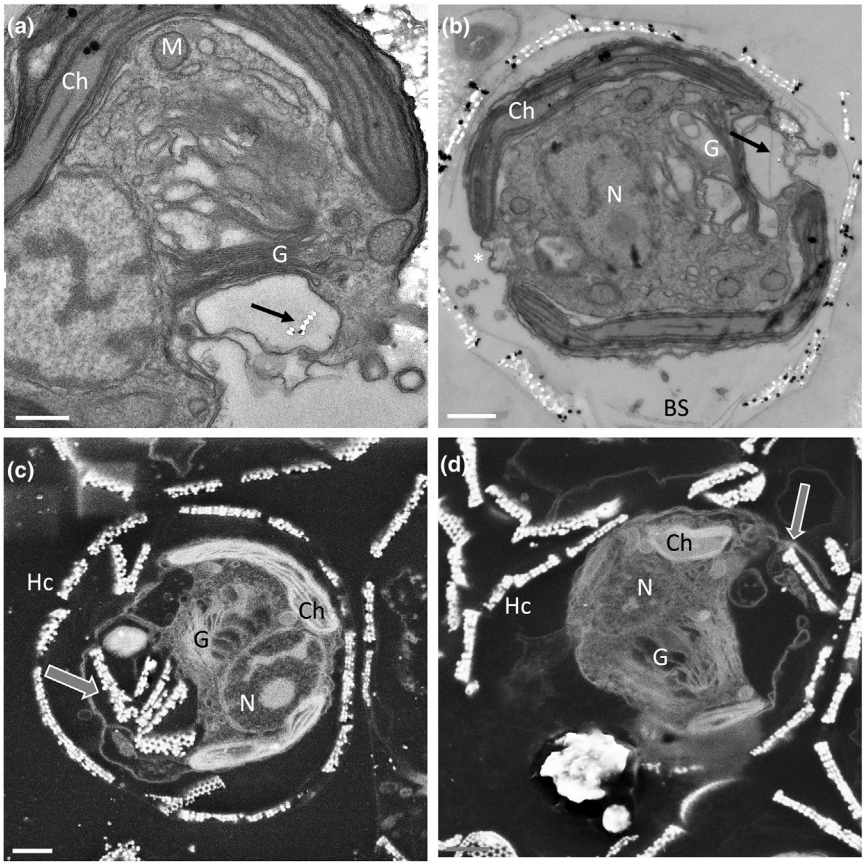

FIGURE 5 Intracellular holococcolith production in *Calcidiscus leptoporus* HOL. (a, b) TEM micrographs showing crystals inside a Golgi-derived vesicle without (a) and with (b) an associated organic scale. (c, d) En bloc backscatter electron micrographs showing mature holococcoliths inside the cell. (c) Intracellular holococcoliths within vesicle prior to secretion. (d) Holococcolith adjacent to the plasmamembrane at the point of being secreted. Black arrow, rhombic crystals within dilated coccolith vesicle; Bs, body scales; Ch, Chloroplast; G, Golgi; Gray arrow, Intracellular holococcoliths; Hc, holococcolith; M, mitochondria; N, Nucleus. Scale bars represent 500 nm (a), 1 μm (b–d).

and *Calyptrosphaera* sp. Significantly, we were able to demonstrate the presence of fully mature intracellular holococcoliths, suggesting that the assembly of the holococcoliths occurs in the vesicle prior to secretion to the extracellular surface.

Holococcogenesis in *Calcidiscus leptoporus* is clearly a highly regulated process despite the relatively simple isotropic crystal composition of holococcoliths. This is evidenced by the precise hexagonal arrangement of two layers of crystallites through contact of neighboring crystal surfaces. Many species have far more complex secondary holococcolith morphologies (Young & Henriksen, 2003). In *C. leptoporus* HOL, the individual calcite crystals appeared to be contacting the organic scale at the apex of the rhombohedron (Figure 4e and see Figure 6c) pointing up from the organic scale along the *c*-axis. The mechanism of nucleation and holococcolith assembly on the organic scale prior to secretion remains unclear. A recent study using focused ion beam-SEM of high-pressure frozen and freeze-substituted *Coccolithus braarudii* HOL and *Calyptosphaera* sp. demonstrated clusters of calcite crystallites in intracellular vesicles that contained one or more organic scales (Ben-Joseph et al., 2023). These presumptive holococcolith vesicles were situated toward the periphery of the flagella pole, the site of holococcolith secretion (see Figure S2a,b). However, ordered synchronous assembly of calcite crystals on the organic scale was not observed, leaving the mechanism of holococcolith assembly, maturation, and secretion unresolved (Ben-Joseph et al., 2023). Further experiments with HOL baseplate scales are warranted to determine the nucleation or scaffolding mechanism of the hexagonally arranged layers of calcite crystallites within the holococcolith vesicle.

The main difference between hetero- and holococcolithogenesis arises during the maturation phase, when the cell utilizes organics like CAP and the cytoskeleton to direct crystal growth and morphogenesis. In one cell, it appeared that numerous holococcoliths were produced simultaneously within the same vacuole. When the holococcoliths were secreted, they were initially attached to the plasma membrane through associations with fibrillar material but eventually became detached and transversed the space between the cell and the surrounding organic matrix before being integrated into the holococcosphere. The mechanism of this transit and integration of holococcoliths into the outer holococcosphere

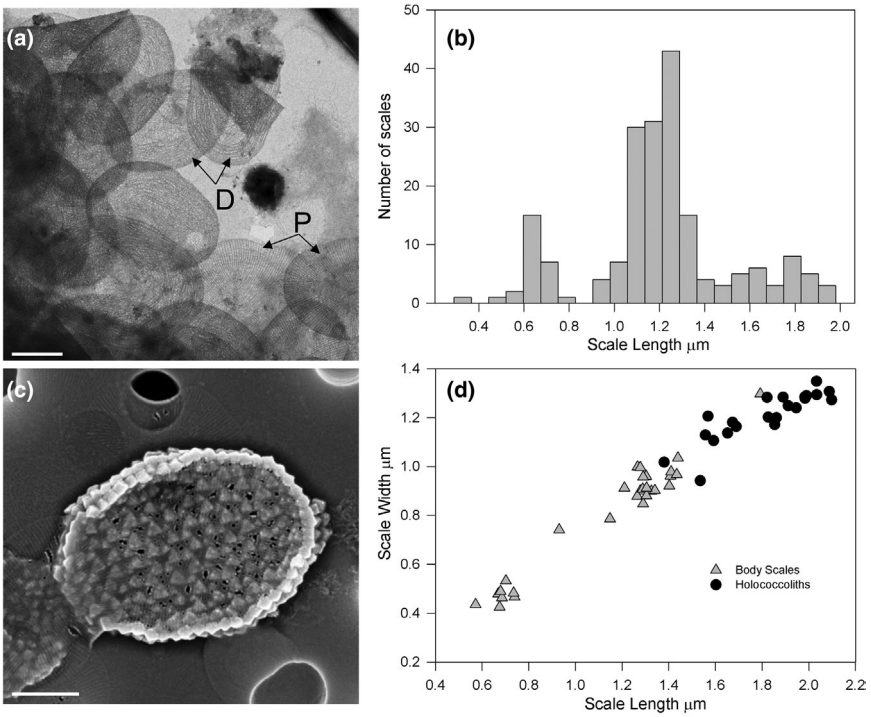

FIGURE 6 Body scales and baseplate scales of *Calcidiscus leptoptous* holococcoliths. (a) TEM micrograph of haploid *C. leptoporus* body scales displaying the different arrangement of fibers: A radial array on the proximal (P) side and a swirl array on the distal (D) side. See also Figure S5. (b) Distribution of organic scale length measured from whole mount negative stain cells in which the calcite was not preserved ($n = 194$). There appear to be 3 size populations with the majority of scales around ~1.2 µm in length. (c) SEM micrograph of overturned holococcolith showing a tightly associated organic layer displaying a fiber pattern similar to the radial array seen on the proximal side of body scales. Scale bars represent 500 nm (a), 1 µm (b). (d) Scatter plot of scale length and width dimensions taken from SEM of mineralized holococcoliths ($n = 22$) and unmineralized body scales ($n = 29$) that confirms the size distribution seen in (b). Mineralized scales fall in a size group category >1.4 µm in length, while unmineralized body scales cluster in a small (~0.65 µm) and larger (~1.3 µm) size group. See also Table S1.

is completely unknown, although amoeboid movements (Taylor et al., 2007) and the haptonema could conceivably play a role.

Baseplate scales for holococcolith production are structurally similar to HOL body scales

Negative staining TEM, conventional TEM, and SEM were used to determine whether there was differentiation among mineralized and unmineralized scales of HOL cells. All organic scales exhibited a slightly oval structure comprising a proximal and distal face with radial and concentric swirled fiber patterns, respectively, bounded by a thickened rim (Figure 6a and Figure S5). The proximal surface of overturned holococcoliths was imaged with SEM, revealing baseplate scales with fiber patterns that matched those of unmineralized body scales (Figure 6c). Although the structure and fibrillar pattern were the same as body scales, the calcified HOL baseplate scales were larger than body scales (1.487 μm ± 0.294 measured with TEM, 1.817 μm ± 0.205 measured with SEM, Table S1, Figure 6d) and corresponded to the dimensions of HET baseplate scales. In alignment with recent theory of the evolution of complex crystal shapes in coccolithophores, the large HOL body scales may have been the precursor to the modern HET baseplate scale (Langer et al., 2021).

The dimensions of unmineralized HOL body scales (Figures 4g, 6a, Figure S5) clustered into two size classes: a small (~0.65 μm) and larger (~1.3 μm) group (Figure 6b,d). This bimodal distribution in scale size had been previously noted in other HOL cells such as *Calyptrosphaera radiata*, *Calyptrosphaera sphaeroidea*, and *Coccolithus pelagicus* (Manton & Leedale, 1963a, 1963b; Noel et al., 2004; Sym & Kawachi, 2000) and could be related to cell size at the time of production, which likely exerts a large, positively correlated influence on coccolith and presumably body scale size (Sucheras-Marx et al., 2022). The size of the body scales and baseplate scales produced immediately following cell division was dramatically constrained but subsequently increased through the growth phase of the cell cycle in line with increasing cell volume, thus giving rise to a range of dimensions observed for scales that accumulate on the cell surface.

Ge sensitivity in 2 N HET cells, but not N HOL cells, supports mechanistic differences in calcification between life phases

Calcidiscus leptoporus HOL exhibited no statistically significant difference in growth rate or coccolith morphology in response to Ge addition up to 20 μM (Figure 7a–e). In contrast, *C. leptoporus* HET grew

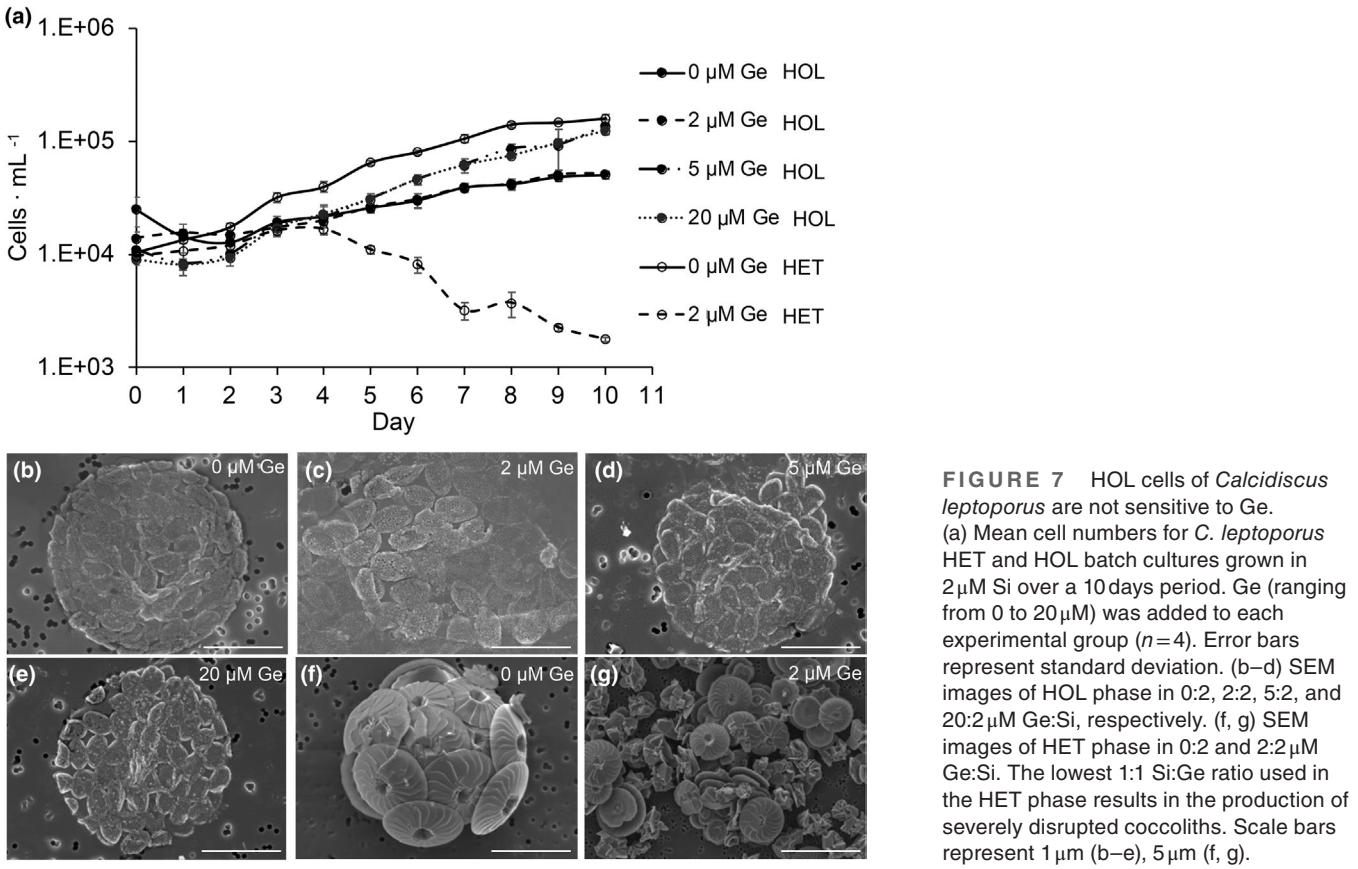

FIGURE 7 HOL cells of *Calcidiscus leptoporus* are not sensitive to Ge. (a) Mean cell numbers for *C. leptoporus* HET and HOL batch cultures grown in 2 μM Si over a 10 days period. Ge (ranging from 0 to 20 μM) was added to each experimental group ($n = 4$). Error bars represent standard deviation. (b–d) SEM images of HOL phase in 0:2, 2:2, 5:2, and 20:2 μM Ge:Si, respectively. (f, g) SEM images of HET phase in 0:2 and 2:2 μM Ge:Si. The lowest 1:1 Si:Ge ratio used in the HET phase results in the production of severely disrupted coccoliths. Scale bars represent 1 μm (b–e), 5 μm (f, g).

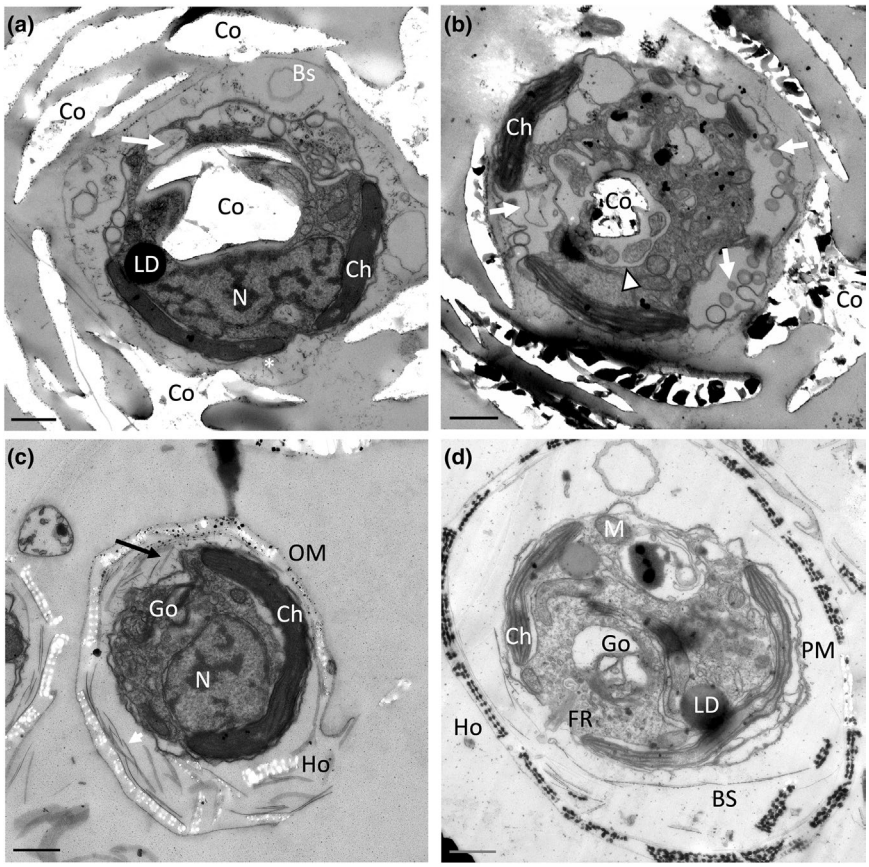

FIGURE 8 Ultrastructural analysis of *Calcidiscus leptoporus* HET and HOL in response to Ge. Cells were grown in media with a 1:0.2 Si:Ge ratio. Diploid *C. leptoporus* under normal (a) and Ge (b) conditions. (a) Bs, body scales; Ch, chloroplast; Co, heterococcolith; LD, lipid droplet; N, nucleus; White arrow, body scale. (b) White arrows, region of vesicles possibly reflecting zone of membrane retrieval (see also Figure S1). Ch, chloroplast; Co, heterococcolith; White arrowhead, compromised CV. Haploid *C. leptoporus* under normal (c) and Ge (d) conditions. Black arrow, fibrillar material; Ch, chloroplast; FR, flagellar root; Go, Golgi; Ho, holococcolith; LD, lipid droplet; M, mitochondria; N, nucleus; OM, organic matrix; PM, plasma membrane; White arrow, body scales. Scale bars represent 1 μm for all panels.

and calcified normally in the absence of Ge, but growth was inhibited after 4 days in the 1:1 Ge:Si treatment (Figure 7a), with newly formed coccoliths produced during the Ge treatment period exhibiting severe malformation that frequently resulted in collapsed coccospheres (Figure 7g). The higher Ge:Si ratio treatments were not conducted for the HET morphotypes following the results of the 1:1 Ge:Si treatment due to the already deleterious effects of the 1:1 treatment after 4 days.

The HET vs. HOL sensitivity to Ge indicates mechanistic differences between hetero- and holococcolith production. Consistent with previous work (Durak et al., 2016), calcification of *Calcidiscus leptoporus* HET was completely disrupted by a 1:1 Si:Ge ratio, while the HOL cells were unaffected even at higher [Ge]. This implies Si uptake via Si transporters (SITs) or SIT-like transporters (SITLs) is not a requirement for holococcolith production. Similar observations were made when comparing the Ge sensitivity of *Coccolithus braarudii* HET and HOL (Langer et al., 2021) and significantly, Langer et al. (2021) were unable to detect SITL expression in the N phase cells. The finding that Si was utilized in heterococcolith production but not in holococcolithogenesis led Langer et al. to propose that the complex crystal morphology of the heterococcoliths was due to the evolution of cellular machinery, such as specific CAPs, that might require Si (Hood et al., 2016; Langer et al., 2021). In *Pleurochrysis carterae* HET, a <20 nm thick organic matrix was observed in association with the surfaces of maturing coccolith calcite, presumably the CAPs that were being utilized for coccolithogenesis (Kadan et al., 2021). Conversely, holococcoliths were comprised of minute calcite rhombohedral crystals influenced largely by inorganic crystal growth. In both cases, nucleation on the organic scale was not affected by Ge treatment or very low Si, but in the case of heterococcoliths, subsequent crystal growth was disrupted by these treatments, suggesting a role for Si in the maturation phase of heterococcolith production (Langer et al., 2021).

In order to further examine the Ge sensitivity of heterococcolith production, we undertook an ultrastructural analysis with TEM of *Calcidiscus leptoporus* HET cells grown in a 1:0.2 Si:Ge medium (Figures 8 and 9, Figure S6). Although nucleation (Figure 9a) and production of coccoliths were evident, this was invariably accompanied by a dramatic distortion of crystal morphology during the maturation of the intracellular coccolith (in over 250 cells observed with intracellular coccoliths; Figure 9b,c, Figure S6). Increased intracellular vacuolization was observed, and the CV membrane no longer appeared to be tightly associated with the mineral surface of the coccolith (Figure 8b, Figure S6). Moreover, membranous structures or cytoplasmic inclusions were observed within the dilated CV (Figure 8b, Figure S6b). Contrastingly, the HOL cell ultrastructure

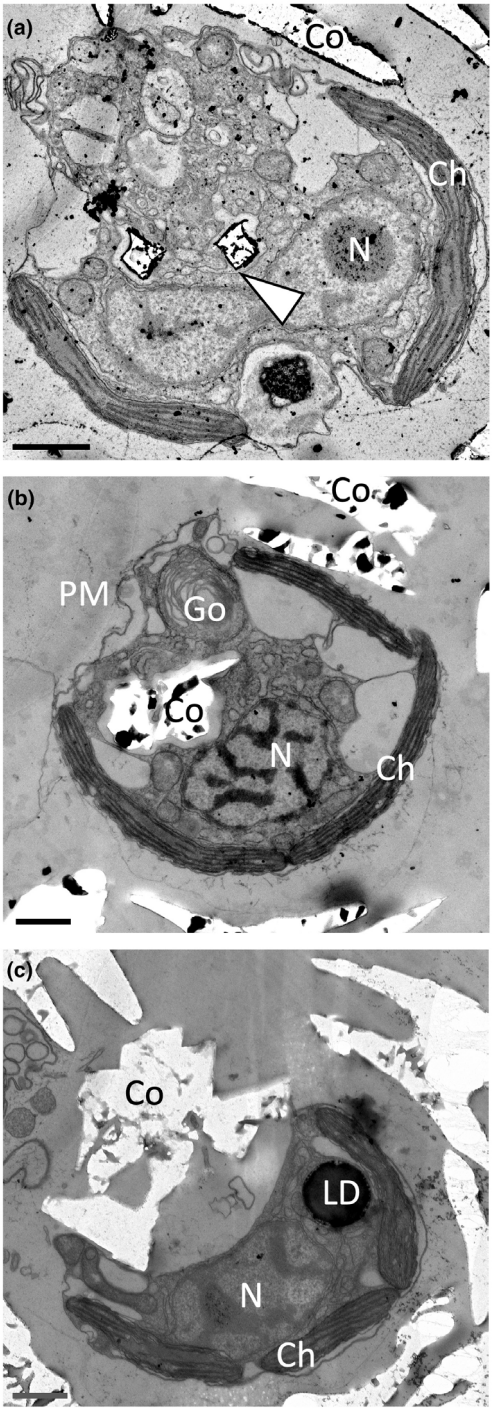

FIGURE 9 Coccolithogenesis of *Calcidiscus leptoporus* HOL in response to Ge. *C. leptoporus* HET cells were grown in media with a 1:0.2 Si:Ge ratio. TEM micrographs show the three stages of coccolithogenesis (a) nucleation white arrow, CV with baseplate scale and developing peripheral protococcolith ring of crystals. (b) maturation, and (c) secretion. Ch, chloroplast; Co, heterococcolith; Go, Golgi; LD, lipid droplet; N, nucleus; PM, plasma membrane. Scale bars represent 1 μm for all panels.

exhibited no signs of disruption when exposed to Ge, and holococcolithogenesis was unaffected (Figure 8c,d).

This TEM analysis confirmed that Ge was affecting the maturation phase in HET cells and not the nucleation of $CaCO_3$. The high degree of Ge-induced disruption of *Calcidiscus leptoporus* HET was apparent through increased vacuolization throughout the cell. Additionally, the CV became dilated and was associated with cytoplasmic intrusions, and it was only loosely associated with the surface of the growing coccolith crystal, which was remarkably similar to the dilated CV of holococcoliths. This supports the need for close contact between the CV membrane and the growing crystal as a critical requirement for heterococcolith morphogenesis, where the CV membrane can both act as a barrier to further crystal growth but could also create ionic nanoenvironments that control growth (Avrahami et al., 2022). Kadan et al. (2021) observed a close association of the CV membrane and maturing crystal in *Pleurochrysis carterae*. Using cryo-electron tomography, they performed native-state imaging without distorting membrane structures (as can easily happen with traditional methods like TEM) and observed that growing crystals were within ~10 nm of the CV membrane. In areas of outward crystal growth, there appeared to be molding by the surrounding membrane, as opposed to crystals that grew inward and displayed smooth crystallographic faces (Kadan et al., 2021). How the CV became so unregulated in response to Ge treatment is not known. However, given the cytoskeleton plays an important role in coccolith morphogenesis (Kadan et al., 2021; Langer et al., 2010), it is possible that Ge treatments may cause loss of cytoskeleton integrity, CV dilation/disorganization, and subsequently the production of malformed coccoliths.

Calcidiscus leptoporus HET and HOL utilize the ER Ca^{2+} transport pathway for calcification

Discovering both holo- and heterococcoliths of *Calcidiscus leptoporus* are produced intracellularly, we hypothesized that HET and HOL cells utilize similar Ca^{2+} transport pathways for calcification. We previously proposed that a likely route for the necessary sustained flux of Ca^{2+} from seawater to the site of calcification is via plasma membrane Ca^{2+} channels allowing rapid Ca^{2+} entry to proximate ER stores that provide a source of Ca^{2+} to the CV (Brownlee et al., 2015). We therefore targeted the highly conserved eukaryote SERCA pump, which has been observed in the *Gephyrocapsa huxleyi* transcriptome (Mackinder et al., 2010; Nam et al., 2019), with thapsigargin to inhibit active Ca^{2+} transport to the site of calcification via the ER. Heterococcolith morphogenesis was significantly disrupted by thapsigargin (Figure 10a,b), with HET cells exhibiting higher frequencies of malformed and rhombic morphologies of coccoliths produced during the treatment period with increasing thapsigargin concentration (Figure 10d). Holococcolith-bearing cells showed the

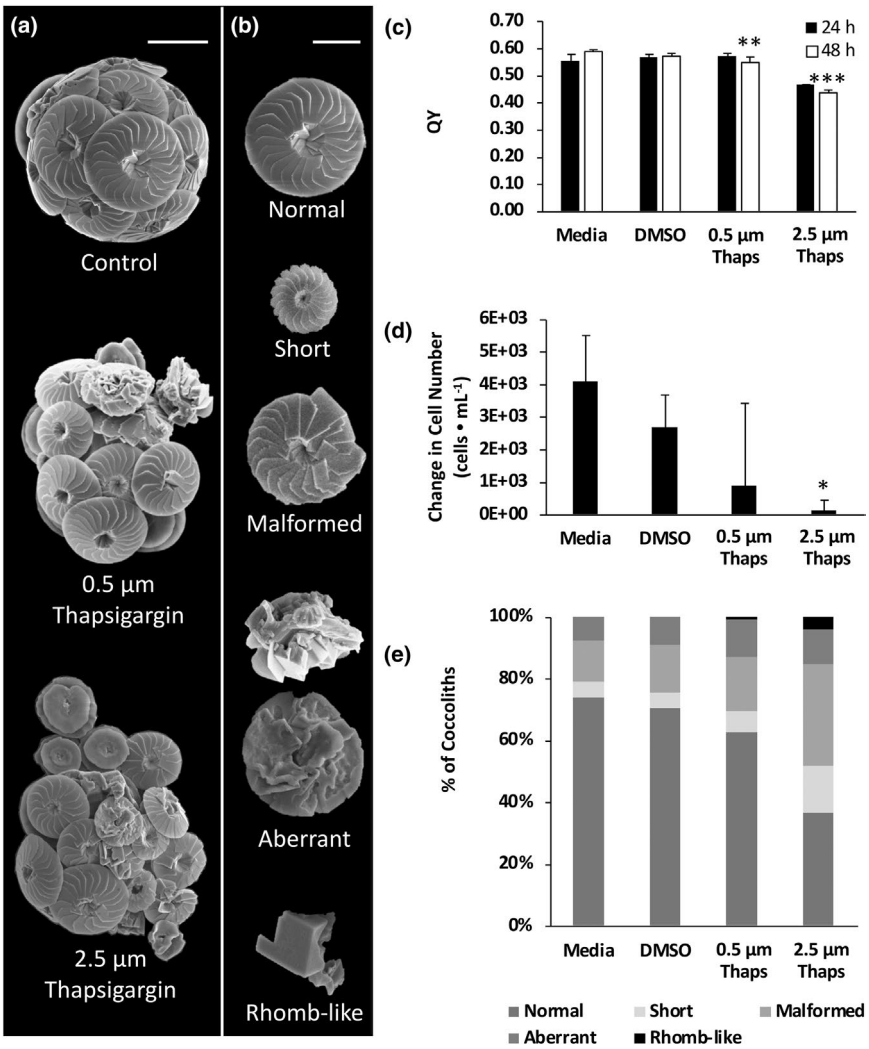

FIGURE 10 *Calcidiscus leptoporus* HET cell division and calcification is disrupted by SERCA inhibitor thapsigargin. (a) Typical control cell (top) and representative images of cells exposed to 0.5 µM and 2.5 µM thapsigargin (middle and bottom) showing the collapsed coccosphere that occurs as a result of the many malformed coccoliths (b) Representative examples of coccolith morphologies used for scoring; Normal, incomplete/short—but otherwise normal morphology, Malformed–minor malformations commonly seen in cultures, Aberrant—coccoliths with significant malformation, and Rhomb-like—cuboidal calcite with no discernable coccolith morphology. (c) Quantum yield (QY) of photosystem II of diploid *C. leptoporus* cells under the different treatment conditions. There were 4 experimental replicates for each treatment, and each replicate was measured three times. The average value was determined within, and between, each replicate. (d) Change in cell number (cells · mL^{-1}) from 24 to 48 h during the treatment incubations. At least 1000 cells were counted per growth flask on each sampling day. (e) Frequencies of coccolith scoring categories in response to thapsigargin. A minimum of 60 cells and 340 heterococcoliths were scored. Error bars = standard deviation for $n = 4$ independent replicates. Scale bars = 2.5 µm. *$p < 0.05$; **$p < 0.01$; ***$p < 0.001$. In each case, the significance is in relation of the treatment to the media control. All statistical comparisons between groups are provided in Table S2.

highest frequencies of weakly or non-calcified cells in the thapsigargin treatments compared to control conditions (Figure 11). The inhibitory effects of thapsigargin on calcification are indicative of a restricted supply of necessary Ca^{2+} ions for proper coccolithogenesis, implying that both life phases utilize the ER (and SERCA pumps) as part of Ca^{2+} transport to the CV. Treatment with the highest thapsigargin concentrations negatively impacted the growth and photosynthetic physiology of both HET and HOL cells (Figure 10c,d and Figure 11e,f), suggesting that at these concentrations, cellular Ca^{2+} homeostasis was irreversibly compromised, leading to cell damage. For the diploid life phase this could be due to the cells requiring an intact coccosphere to divide (Walker et al., 2018). However, we cannot rule out the possibility that thapsigargin, while being used at sub-lethal concentrations, impacted overall Ca^{2+} transport and cellular function (as evidenced by lower *Fv*/*Fm* values) therefore disrupting other aspects of cellular metabolism and/or cell division.

Despite having very different coccolith morphologies, these data demonstrate the biomineralization systems of haploid and diploid coccolithophores share the same fundamental transport mechanisms for coccolith

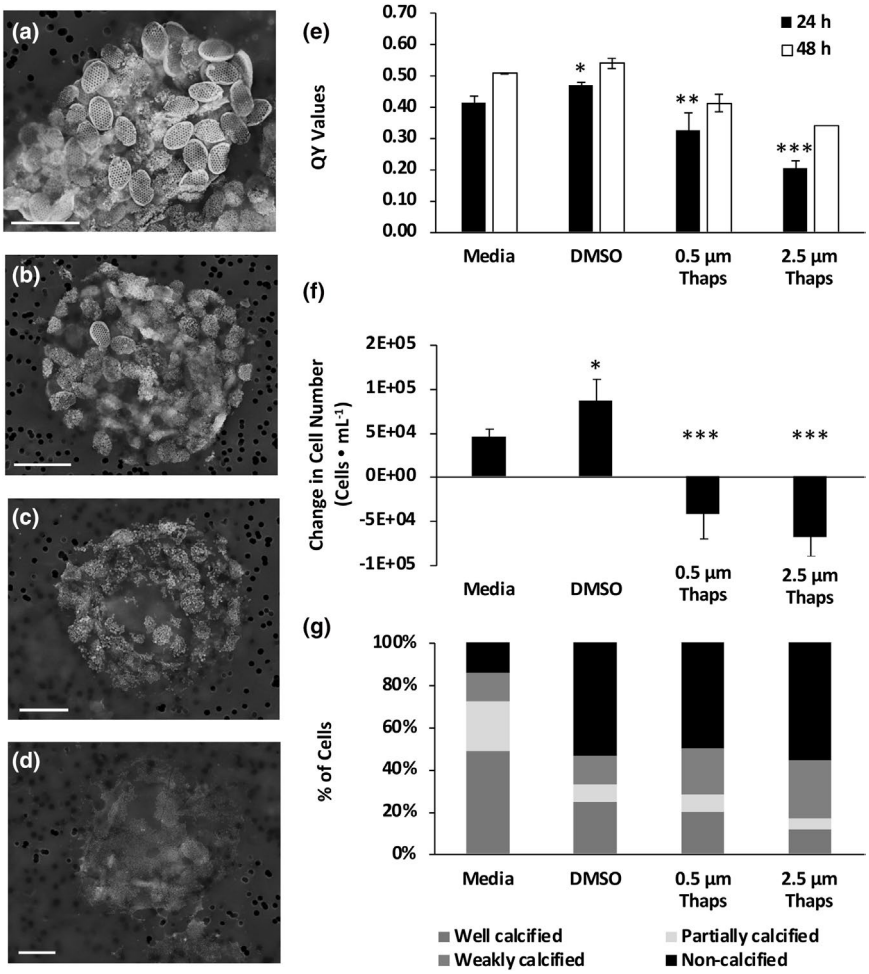

FIGURE 11 *Calcidiscus leptoporus* HOL cell division and calcification disrupted by SERCA inhibitor thapsigargin. (a–d) Representative examples of coccosphere calcification when grown in (a) normal control media, (b) DMSO, (c) 0.5 µM thapsigargin, and (d) 2.5 µM thapsigargin treatments. (e) Quantum yield (QY) of photosystem II of haploid *C. leptoporus* in response to thapsigargin treatment. There were 4 experimental replicates for each treatment, and each replicate was measured three times. The average value was determined within, and between, each replicate. (f) Change in cell number (cells · mL^{-1}) from 24 to 48 h across treatments. At least 1000 cells were counted per growth flask on each sampling day. (g) Frequencies of coccolith morphologies in response to thapsigargin treatment. A minimum of 60 cells were scored. See methods for a description of the different categories. Error bars = standard deviation for $n = 4$ independent replicates. Scale bars = 5 µm. *$p < 0.05$; **$p < 0.01$; ***$p < 0.001$. In each case, the significance is in relation to the treatment of the media control. All statistical comparisons between groups are provided in Table S2.

production. Intracellular calcification requires an efficient Ca^{2+} transport pathway to the mineralizing vesicle while minimizing fluctuations in $[Ca^{2+}]_{cyt}$. Due to this high Ca^{2+} requirement, coccolithophores likely utilize a wide variety of pumps and channels (Berry et al., 2002; Mackinder et al., 2010). Although Ca^{2+} transport in coccolithophores remains poorly characterized, our results supported Ca^{2+} accumulation in the ER through a SERCA pump, and through this endomembrane route, Ca^{2+} could be delivered to localized regions such as the prominent ER membranes that are intimately associated with the CV (Berry et al., 2002; Brownlee et al., 2015; Drescher et al., 2012; Taylor et al., 2007, 2017). The upregulation in genes associated with endomembrane Ca^{2+} transporters in actively calcifying cells (Mackinder et al., 2011) supported an ER-based route for Ca^{2+} supply to the coccolith vesicle.

A word of caution when using DMSO

We detected some DMSO sensitivity in both *Calcidiscus leptoporus* HET and HOL cells when exposed to the carrier solvent DMSO alone (Figures 10 and 11). In *C. leptoporus* HET, there was a small but not statistically significant reduction in cell growth when exposed to 0.025% v/v DMSO, and in HOL cells, there was a significant decrease in well-calcified cells in response to 0.05% v/v DMSO compared to the media control treatment (Figure 10g). Because photosynthetic physiology was unaffected in both cases, there must have been a more subtle effect of the solvent on cell physiology. Coccolithophores are known to produce elevated levels of methyl sulfur-related products, and *Gephyrocapsa huxleyi* can produce and store high intracellular levels of dimethyl sulfoniopropionate (DMSP)—up to 400 mM

(Seyedsayamdost et al., 2011; Taylor et al., 2017). Perhaps unsurprisingly, *G. huxleyi* cells are unaffected by treatments up to 0.5% DMSO (Langer et al., 2010). Other coccolithophore species such as *Coccolithus braarudii* and *Scyphosphaera apsteinii* also appear to be insensitive to the addition of up to 0.01%vol DMSO with no obvious effects on growth or malformations of coccoliths (Langer et al., 2023). Nevertheless, although DMSO (~10% v/v) is widely used as a cellular cryoprotectant for frozen storage, much lower concentrations (0.1–1% v/v) have been shown to affect a range of cellular processes in animal cells (Awan et al., 2020), including cell division, possibly through effects on spindle formation (Kang et al., 2020; Li et al., 2016; Vesey et al., 1991), and a decrease in the growth of *Arabidopsis thaliana* roots was observed in treatments of 0.5%vol DMSO (Urbina et al., 2006). Moreover, Santos et al. (2003) summarized multiple studies that reported decreases in intracellular Ca^{2+} levels in response to DMSO in various systems. The mechanism for DMSO interaction with Ca^{2+} stores at these high levels has not been explained. We conclude that DMSO tolerance may vary quite widely among coccolithophores and the phases of their life histories and, therefore, should be carefully assessed on a case-by-case basis for each species when using this solvent for experimental manipulations.

CONCLUSIONS

This study provides a detailed ultrastructural analysis of *Calcidiscus leptoporus* for both HET and HOL morphotypes and life phases (see Figure S7 for a schematic diagram summarizing key findings). Moreover, we have provided definitive evidence for intracellular production and maturation of holococcoliths within Golgi-derived vesicles in *C. leptoporus* prior to secretion. Evidently, heterococcolith and holococcolith biomineralization mechanisms have more in common than previously appreciated. Based on these observations, we conclude that production of holococcoliths follows a similar sequence as in heterococcolithogenesis: (1) nucleation of calcite crystal rhombs arranged with specific crystallographic orientations on an organic scale, (2) growth of calcite crystals through predominantly inorganic processes in a dilated vacuole (i.e., limited morphological control on crystal growth), followed by (3) termination of crystal growth and (4) secretion of a mature holococcolith onto the cell surface and incorporation into the coccosphere. Further evidence that both *C. leptoporus* HET and HOL cells utilize the same intracellular calcification pathway is their sensitivity to the SERCA pump inhibitor thapsigargin. This strongly supports a model of ER-based Ca^{2+} transport required to supply the flux of Ca^{2+} necessary to maintain a sufficient saturation state at the site of intracellular calcification. Importantly, there are clear differences such as the dilated CV for holococcoliths compared to the tight association of the CV membrane with heterococcoliths, which has profound consequences for coccolith crystal growth and morphology. Additionally, our results have provided evidence that both holococcoliths and heterococcoliths nucleate on a morphologically similar organic scale in *C. leptoporus*. This is consistent with the recently proposed theory that calcification first evolved in a HOL cell, with heterococcolith complexity arising from the evolution of additional cellular machinery including CAP and tight association of the CV membrane and calcite surface. Although this study provides insights into the cellular mechanisms underlying holococcolithogenesis, more research is clearly needed to fully understand how holococcoliths are assembled, secreted, and organized into the extracellular layer.

AUTHOR CONTRIBUTIONS

Erin M. Meyer: Conceptualization (equal); formal analysis (equal); investigation (lead); methodology (lead); writing – original draft (lead); writing – review and editing (supporting). **Alison R. Taylor:** Conceptualization (equal); formal analysis (equal); funding acquisition (lead); investigation (supporting); methodology (supporting); supervision (lead); writing – original draft (supporting); writing – review and editing (lead).

ACKNOWLEDGMENTS

We thank Dr. Gerald Langer for helpful discussions during this study. The work was supported by NSF GEO-NERC grant 1638838 and Natural Environment Research Council grant NE/N011708/1 to ART. Extensive use of the Richard M. Dillaman Biological Imaging Facility at the University of North Carolina Wilmington was supported by NSF MRI 1229024 and NSF MRI 1828053.

ORCID

Alison R. Taylor https://orcid.org/0000-0002-2275-0246

REFERENCES

Andersson, M. P., Hem, C. P., Schultz, L. N., Nielsen, J. W., Pedersen, C. S., Sand, K. K., Okhrimenko, D. V., Johnsson, A., & Stipp, S. L. (2014). Infrared spectroscopy and density functional theory investigation of calcite, chalk, and coccoliths–do we observe the mineral surface? *The Journal of Physical Chemistry*, *A118*, 10720–10729.

Avrahami, E. M., & Frada, M. J. (2020). Detection of phagotrophy in the marine phytoplankton group of the coccolithophores (Calcihaptophycidae, Haptophyta) during nutrient-replete and phosphate-limited growth. *Journal of Phycology*, *56*(4), 1103–1108.

Avrahami, E. M., Houben, L., Aram, L., & Gal, A. (2022). Complex morphologies of biogenic crystals emerge from anisotropic growth of symmetry-related facets. *Science*, *376*, 312–316.

Awan, M., Buriak, I., Fleck, R., Fuller, B., Goltsev, A., Kerby, J., Lowdell, M., Mericka, P., Petrenko, A., Petrenko, Y., Rogulska,

O., Stolzing, A., & Stacey, G. N. (2020). Dimethyl sulfoxide: A central player since the dawn of cryobiology, is efficacy balanced by toxicity? *Regenerative Medicine*, *15*, 1463–1491.

Baumann, K., Böckel, B., & Frenz, M. (2004). Coccolith contribution to South Atlantic carbonate sedimentation. In H. R. Thierstein & J. R. Young (Eds.), *Coccolithophores: From molecular processes to global impact* (pp. 367–402). Springer.

Bendif, E. M., Probert, I., Archontikis, O. A., Young, J. R., Beaufort, L., Rickaby, R. E., & Filatov, D. (2023). Rapid diversification underlying the global dominance of a cosmopolitan phytoplankton. *The ISME Journal*, *17*(4), 630–640.

Ben-Joseph, O., de Haan, D., Rechav, K., Shimoni, E., Levin-Zaidman, S., Langer, G., Probert, I., Wheeler, G. L., & Gal, A. (2023). Crystallization of coccolith calcite at different life-cycle phases exhibits distinct degrees of cellular confinement. *Small Structures*, *4*(7), 2200353. https://doi.org/10.1002/sstr.202200353

Berry, L., Taylor, A. R., Lucken, U., Ryan, K. P., & Brownlee, C. (2002). Calcification and inorganic carbon acquisition in coccolithophores. *Functional Plant Biology*, *29*, 289–299.

Beuvier, T., Probert, I., Beaufort, L., Sucheras-Marx, B., Chushkin, Y., Zontone, F., & Gibaud, A. (2019). X-ray nanotomography of coccolithophores reveals that coccolith mass and segment number correlate with grid size. *Nature Communications*, *10*, 751.

Billard, C., & Inouye, I. (2004). What is new in coccolithophore biology? In H. R. Thierstein & J. R. Young (Eds.), *Coccolithophores: From molecular processes to global impact* (pp. 1–29). Springer.

Braarud, T., Deflandre, G., Halldal, P., & Kamptner, E. (1955). Terminology, nomenclature, and systematics of the Coccolithophoridae. *Micropaleontology*, *1*(2), 157–159.

Brownlee, C., Wheeler, G. L., & Taylor, A. R. (2015). Coccolithophore biomineralization: New questions, new answers. *Seminars in Cell & Developmental Biology*, *46*, 11–16.

Brzezinski, M. A., Alldredge, A. L., & O'bryan, L. M. (1997). Silica cycling within marine snow. *Limnology and Oceanography*, *42*, 1706–1713.

Brzezinski, M. A., & Nelson, D. M. (1995). The annual silica cycle in the Sargasso Sea near Bermuda. *Deep-Sea Research Part I-Oceanographic Research Papers*, *42*, 1215–1237.

Cros, L., Fortuño, J. M., & Estrada, M. (2013). Elemental composition of coccoliths: Mg/Ca relationships. *Scientia Marina*, *77*, 63–67.

D'Amario, B., Ziveri, P., Grelaud, M., Oviedo, A., & Kraij, M. (2017). Coccolithophore haploid and diploid distribution patterns in the Mediterranean Sea: Can a haplo-diploid life cycle be advantageous under climate change? *Journal of Plankton Research*, *39*, 781–794.

Daniels, C. J., Poulton, A. J., Young, J. R., Esposito, M., Humphreys, M. P., Ribas-Ribas, M., Tynan, E., & Tyrrell, T. (2016). Species-specific calcite production reveals *Coccolithus pelagicus* as the key calcifier in the Arctic Ocean. *Marine Ecology Progress Series*, *555*, 29–47.

Drescher, B., Dillaman, R. M., & Taylor, A. R. (2012). Coccolithogenesis in *Scyphosphaera apsteinii* (Prymnesiophyceae). *Journal of Phycology*, *48*, 1343–1361.

Durak, G. M., Taylor, A. R., Walker, C. E., Probert, I., De Vargas, C., Audic, S., Schroeder, D., Brownlee, C., & Wheeler, G. L. (2016). A role for diatom-like silicon transporters in calcifying coccolithophores. *Nature Communications*, *7*, 10543.

Eikrem, W., Medlin, L. K., Henderiks, J., Rokitta, S., Rost, B., Probert, I., Throndsen, J., & Edvardsen, B. (2016). Haptophyta. In J. M. Archibald (Ed.), *Handbook of the protists*. Springer International Publishing.

Eyal, Z., Krounbi, L., Ben Joseph, O., Avrahami, E. M., Pinkas, I., Peled-Zehavi, H., & Gal, A. (2022). The variability in the structural and functional properties of coccolith base plates. *Acta Biomaterialia*, *148*, 336–344.

Fowler, N., Tomas, C., Baden, D., Campbell, L., & Bourdelais, A. (2015). Chemical analysis of *Karenia papilionacea*. *Toxicon*, *101*, 85–91.

Frada, M., Percopo, I., Young, J., Zingone, A., De Vargas, C., & Probert, I. (2009). First observations of heterococcolithophore-holococcolithophore life cycle combinations in the family Pontosphaeraceae (Calcihaptophycideae, Haptophyta). *Marine Micropaleontology*, *71*, 20–27.

Frada, M., Probert, I., Allen, M. J., Wilson, W. H., & De Vargas, C. (2008). The "Cheshire cat" escape strategy of the coccolithophore *Emiliania huxleyi* in response to viral infection. *Proceedings of the National Academy of Sciences of the United States of America*, *105*, 15944–15949.

Frada, M. J., Rosenwasser, S., Ben-Dor, S., Shemi, A., Sabanay, H., & Vardi, A. (2017). Morphological switch to a resistant subpopulation in response to viral infection in the bloom-forming coccolithophore *Emiliania huxleyi*. *PLoS Pathogens*, *13*, 17.

Geisen, M., Billard, C., Broerse, A. T. C., Cros, L., Probert, I., & Young, J. R. (2002). Life-cycle associations involving pairs of holococcolithophorid species: Intraspecific variation or cryptic speciation? *European Journal of Phycology*, *37*, 531–550.

Green, J. C., Course, P. A., & Tarran, G. A. (1996). The life-cycle of *Emiliania huxleyi*: A brief review and a study of relative ploidy levels analysed by flow cytometry. *Journal of Marine Systems*, *9*, 33–44.

Hood, M. A., Leemreize, H., Scheffel, A., & Faivre, D. (2016). Lattice distortions in coccolith calcite crystals originate from occlusion of biomacromolecules. *Journal of Structural Biology*, *196*, 147–154.

Houdan, A., Billard, C., Marie, D., Not, F., Sáez, A. G., Young, J. R., & Probert, I. (2004). Holococcolithophore-heterococcolithophore (Haptophyta) life cycles: Flow cytometric analysis of relative ploidy levels. *Systematics and Biodiversity*, *1*, 453–465.

Houdan, A., Probert, I., Zatylny, C., Veron, B., & Billard, C. (2006). Ecology of oceanic coccolithophores. I. Nutritional preferences of the two stages in the life cycle of *Coccolithus braarudii* and *Calcidiscus leptoporus*. *Aquatic Microbial Ecology*, *44*, 291–301.

Iglesias-Rodriguez, M. D., Brown, C. W., Doney, S. C., Kleypas, J., Kolber, D., Kolber, Z., Hayes, P. K., & Falkowski, P. G. (2002). Representing key phytoplankton functional groups in ocean carbon cycle models: Coccolithophorids. *Global Biogeochemical Cycles*, *16*, 20.

Kadan, Y., Tollervey, F., Varsano, N., Mahamid, J., & Gal, A. (2021). Intracellular nanoscale architecture as a master regulator of calcium carbonate crystallization in marine microalgae. *Proceedings of the National Academy of Sciences of the United States of America*, *118*, e2025670118.

Kang, M. H., You, S. Y., Hong, K., & Kim, J. H. (2020). DMSO impairs the transcriptional program for maternal-to-embryonic transition by altering histone acetylation. *Biomaterials*, *230*, 119604.

Klaveness, D. (1973). The microanatomy of *Calyptrosphaera sphaeroidea*, with some supplementary observations in the motile stage of *Coccolithus pelagicus*. *Nordic Journal of Botany*, *20*, 151–162.

Klaveness, D., & Paasche, E. (1971). Two different *Coccolithus-huxleyi* cell types incapable of coccolith formation. *Archiv Fur Mikrobiologie*, *75*, 382–385.

Laguna, R., Romo, J., Read, B. A., & Wahlund, T. M. (2001). Induction of phase variation events in the life cycle of the marine coccolithophorid *Emiliania huxleyi*. *Applied and Environmental Microbiology*, *67*, 3824–3831.

Langer, G., De Nooijer, L. J., & Oetjen, K. (2010). On the role of the cytoskeleton in coccolith morphogenesis: The effect of cytoskeleton inhibitors. *Journal of Phycology*, *46*, 1252–1256.

Langer, G., Probert, I., Cox, M. B., Taylor, A., Harper, G. M., Brownlee, C., & Wheeler, G. (2023). The effect of cytoskeleton inhibitors on coccolith morphology in *Coccolithus braarudii* and *Scyphosphaera apsteinii*. *Journal of Phycology*, *59*, 87–96.

Langer, G., Taylor, A. R., Walker, C. E., Meyer, E. M., Ben Joseph, O., Gal, A., Harper, G. M., Probert, I., Brownlee, C., & Wheeler, G. L. (2021). Role of silicon in the development of complex crystal shapes in coccolithophores. *New Phytologist*, *231*, 1845–1857.

Li, X., Wang, Y. K., Song, Z. Q., Du, Z. Q., & Yang, C. X. (2016). Dimethyl sulfoxide perturbs cell cycle progression and spindle organization in porcine meiotic oocytes. *PLoS ONE*, *11*, e0158074.

Mackinder, L., Wheeler, G., Schroeder, D., Von Dassow, P., Riebesell, U., & Brownlee, C. (2011). Expression of biomineralization-related ion transport genes in *Emiliania huxleyi*. *Environmental Microbiology*, *13*, 3250–3265.

Mackinder, L., Wheeler, G., Schroeder, D., Riebesell, U., & Brownlee, C. (2010). Molecular mechanisms underlying calcification in coccolithophores. *Geomicrobiology Journal*, *27*, 585–595.

Manton, I., & Leedale, G. F. (1963a). Observations on the fine structure of *Prymnesium parvum carter*. *Archiv für Mikrobiologie*, *45*, 285–303.

Manton, I., & Leedale, G. F. (1963b). Observations on the microanatomy of *Crystallolithus hyalinus* Gaarder and Markali. *Archiv für Mikrobiologie*, *47*, 115–136.

Manton, I., & Leedale, G. F. (1969). Observations on the microanatomy of *Coccolithus pelagicus* and *Cricosphaera carterae*, with special reference to the origin and nature of coccoliths and scales. *Journal of the Marine Biological Association of the United Kingdom*, *49*, 1–16.

Marsh, M. E. (1999). Coccolith crystals of *Pleurochrysis carterae*: Crystallographic faces, organization, and development. *Protoplasma*, *207*, 54–66.

Marzec, B., Walker, J. M., Panagopoulou, M., Jhons, Y., Clare, D., Wheeler, A., Shaver, M. P., & Nudelman, F. (2019). Three-dimensional architecture and surface functionality of coccolith base plates. *Journal of Structural Biology*, *208*, 127–136.

Mordecai, G. J., Verret, F., Highfield, A., & Schroeder, D. C. (2017). Schrodinger's Cheshire cat: Are haploid *Emiliania huxleyi* cells resistant to viral infection or not? *Viruses-Basel*, *9*, 17.

Nam, O., Park, J. M., Lee, H., & Jin, E. (2019). De novo transcriptome profile of coccolithophorid alga *Emiliania huxleyi* CCMP371 at different calcium concentrations with proteome analysis. *PLoS ONE*, *14*(8), e0221938.

Noel, M. H., Kawachi, M., & Inouye, I. (2004). Induced dimorphic life cycle of a coccolithophorid, *Calyptrosphaera sphaeroidea* (Prymnesiophyceae, Haptophyta). *Journal of Phycology*, *40*, 112–129.

Parke, M., & Adams, I. (1960). The motile (*Crystallolithus hyalinus* Gaarder & Markali) and non-motile phases in the life history of *Coccolithus pelagicus* (Wallich). *Journal of the Marine Biological Association of the United Kingdom*, *39*, 263–274.

Renaud, S., & Klaas, C. (2001). Seasonal variations in the morphology of the coccolithophore *Calcidiscus leptoporus* off Bermuda (N. Atlantic). *Journal of Plankton Research*, *23*(8), 779–795.

Reynolds, E. S. (1963). The use of lead citrate at high pH as an electron-opaque stain in electron microscopy. *Journal of Cell Biology*, *17*, 208–212.

Rowson, J. D., Leadbeater, B. S. C., & Green, J. C. (1986). Calcium-carbonate deposition in the motile (Crystallolithus) phase of *Coccolithus-pelagicus* (Prymnesiophyceae). *British Phycological Journal*, *21*, 359–370.

Santos, N. C., Figueira-Coelho, J., Martins-Silva, J., & Saldanha, C. (2003). Multidisciplinary utilization of dimethyl sulfoxide: Pharmacological, cellular, and molecular aspects. *Biochemical Pharmacology*, *65*, 1035–1041.

Seyedsayamdost, M. R., Case, R. J., Kolter, R., & Clardy, J. (2011). The Jekyll-and-Hyde chemistry of *Phaeobacter gallaeciensis*. *Nature Chemistry*, *3*, 331–335.

Silva, A., Palma, S., Oliveria, P. B., & Moita, M. T. (2009). *Calcidiscus quadriperforatus* and *Calcidiscus leptoporus* as oceanographic tracers in Lisbon Bay (Portugal). *Estuarine, Coastal and Shelf Science*, *81*(3), 333–344.

Stoll, H. M., Ziveri, P., Geisen, M., Probert, I., & Young, J. R. (2002). Potential and limitations of Sr/Ca ratios in coccolith carbonate: New perspectives from cultures and monospecific samples from sediments. *Philosophical Transactions of the Royal Society A*, *360*, 719–747.

Subhas, A. V., Rollins, N. E., Berelson, W. M., Erez, J., Ziveri, P., Langer, G., & Adkins, J. F. (2018). The dissolution behavior of biogenic calcites in seawater and a possible role for magnesium and organic carbon. *Marine Chemistry*, *205*, 100–112.

Sucheras-Marx, B., Viseur, S., Walker, C. E., Beaufort, L., Probert, I., & Bolton, C. (2022). Coccolith size rules-what controls the size of coccoliths during coccolithogenesis? *Marine Micropaleontology*, *170*, 102080.

Sym, S., & Kawachi, M. (2000). Ultrastructure of *Calyptrosphaera radiata*, sp. nov. (Prymnesiophyceae, Haptophyta). *European Journal of Phycology*, *35*, 283–293.

Taylor, A. R., Brownlee, C., & Wheeler, G. (2017). Coccolithophore cell biology: Chalking up progress. *Annual Review of Marine Science*, *9*, 283–310.

Taylor, A. R., Russell, M. A., Harper, G. M., Collins, T. F. T., & Brownlee, C. (2007). Dynamics of formation and secretion of heterococcoliths by *Coccolithus pelagicus* ssp. *braarudii*. *European Journal of Phycology*, *42*, 125–136.

Urbina, D. C., Silva, H., & Meisel, L. A. (2006). The Ca^{2+} pump inhibitor, thapsigargin, inhibits root gravitropism in *Arabidopsis thaliana*. *Biological Research*, *39*, 289–296.

de Vargas, C., Aubry, M.-P., Probert, I., & Young, J. (2007). Origin and evolution of coccolithophores: From coastal hunters to oceanic farmers. In P. Falkowski & A. Knoll (Eds.), *Evolution of primary producers in the sea* (pp. 251–286). Elsevier Academic Press.

Vesey, D. A., Cunningham, J. M., Selden, A. C., Woodman, A. C., & Hodgson, H. J. F. (1991). Dimethyl-sulfoxide induces a reduced growth-rate, altered cell morphology and increased epidermal-growth-factor binding in HEP G2 cells. *Biochemical Journal*, *277*, 773–777.

de Vries, J., Monteiro, F., Wheeler, G., Poulton, A., Godrijan, J., Cerino, F., Malinverno, E., Langer, G., & Brownlee, C. (2021). Haplo-diplontic life cycle expands coccolithophore niche. *Biogeosciences*, *18*, 1161–1184.

Walker, C. E., Taylor, A. R., Langer, G., Durak, G. M., Heath, S., Probert, I., Tyrrell, T., Brownlee, C., & Wheeler, G. L. (2018). The requirement for calcification differs between ecologically important coccolithophore species. *New Phytologist*, *220*, 147–162.

Walker, J. M., & Langer, G. (2021). Coccolith crystals: Pure calcite or organic-mineral composite structures? *Acta Biomaterialia*, *125*, 83–89.

Westbroek, P., Young, J. R., & Linschooten, K. (1989). Coccolith production (biomineralization) in the marine alga *Emiliania huxleyi*. *Journal of Protozoology*, *36*, 368–373.

Young, J. R. (1987). Possible functional interpretations of coccolith morphology. *Abhandlungen der Geologische Bundesanstalt*, *39*, 305–313.

Young, J. R. (1989). Observations on heterococcolith rim structure and its relationship to developmental processes. In J. A. Crux & S. E. V. Heck (Eds.), *Nannofossils and their applications* (pp. 1–20). Ellis Horwood.

Young, J. R., Cros, L., Kleine, A., Sprengel, C., Probert, I., & Ostergaard, J. B. (2003). *A guide to extant coccolithophore taxonomy*. International Nannoplankton Association.

Young, J. R., Davis, S. A., Bown, P. R., & Mann, S. (1999). Coccolith ultrastructure and biomineralisation. *Journal of Structural Biology*, *126*, 195–215.

Young, J. R., Didymus, J. M., Bown, P. R., Prins, B., & Mann, S. (1992). Crystal assembly and phylogenetic evolution in heterococcoliths. *Nature*, *356*, 516–518.

Young, J. R., Geisen, M., & Probert, I. (2005). Review of selected aspects of coccolithophore biology with implications for paleobiodiversity estimation. *Micropaleontology*, *51*, 267–288.
Young, J. R., & Henriksen, K. (2003). Biomineralization within vesicles: The calcite of coccoliths. *Biomineralization*, *54*, 189–215.

SUPPORTING INFORMATION

Additional supporting information can be found online in the Supporting Information section at the end of this article.

Figure S1. Zone of membrane exchange in *Calcidiscus leptoporus* HET. Representative examples of TEM and en bloc SEM images of cells in which a zone of large vesicles (~50 nm diameter) at various stages of fusion and/or retrieval. (a) Glancing TEM section through peripheral region of cell showing a patch of well-ordered vesicles (pale pink color) just below the plasma membrane. (b) TEM cross section of cell with internal coccolith and part of the vesicle rich region apparent. (c) Backscatter image of en bloc sectioned cells showing cell with surrounding calcite coccoliths, internal nucleus, chloroplasts, prominent Golgi, and region of peripheral vesicles (pink). (d) inverted image of en bloc SEM image in (c) giving a more conventional TEM-like appearance. Scale bars: (a, b) 1 μm, (c, d) 5 μm.

Figure S2. Ultrastructure of *Calcidiscus leptoporus* HOL. (a) TEM of whole cell prepared with an unmodified protocol, so no calcite is preserved. Nucleus (N) with nuclear pores (white arrows), chloroplasts (Cl) with immersed pyrenoid (Py), mitochondria (Mt), plasma membrane (Pm) and prominent Golgi body (G) with gray arrow indicating the cis-trans progression of the Golgi cisternae with a dilated trans-Golgi cisternae adjacent to the flagella pole of the cell. Flagella root (white dotted rectangle). Space between the cell and outer layer of scales is indicated by double headed arrow. (b) Detail of the flagella pole of a cell showing basal body (Ba), elements of the flagellar root (Rt) and adjacent dilated trans-Golgi vesicle with organic scale (Sc). (c) Detail of cell showing arrangement of extracellular components; Plasma membrane (Pm) with fibrillar material (Fm) that allows for focal adhesions to innermost body scales (Sc) that are arranged in multiple layers that are enclosed by a layer of diffuse organic material (Om). Scale bars: (a) 1 μm, (b, c) 0.5 μm.

Figure S3. Prolific scale production in *Calcidiscus leptoporus* HOL. (a) TEM micrograph showing single prominent cis to trans-Golgi body (gray arrow) with scale being produced in the trans-Golgi cisternae for release to the flagellar pole cell surface. (b) Detail of trans-Golgi as indicated by the white dotted area in (a). (c) Tangential section through trans-Golgi cisternae with scale (dotted white line). Scale Bars: (a, c) 1 μm, (b) 0.5 μm.

Figure S4. Large vacuoles observed in *Calcidiscus leptoporus* HOL. (a–d) TEM micrographs showing a prominent vacuolar space observed in *Calcidiscus leptoporus* HOL cells. Bs, body scales; Ch, chloroplast; G, Golgi; Hc, holococcolith; M, mitochondria; N, nucleus; Om, extracellular layer or organic material; Pm, plasma membrane; V, vacuole. Scale Bars: (c) 1 μm.

Figure S5. *Calcidiscus leptoporus* HOL organic scales. (a) TEM micrograph of a glancing section through the extracellular region of a cell showing calcified scales over the top of uncalcified scales. The organic layer over the coccosphere is also apparent. (b) Whole mount of a decalcified cell showing organic scales of the same morphology but different sizes. (c) TEM micrograph showing cross section of a holococcolith (calcite crystals have dissolved leaving holes in the resin) with associated organic scale. Bs, baseplate scale of holococcolith; Om, outer layer of amorphous organic material. Scale bars: (a) 0.5 μm, (b) 1 μm, (c) 0.2 μm.

Figure S6. Unregulated calcification in *Calcidiscus leptoporus* HET in response to germanium. (a–c) En bloc SEM backscattered electron images (left) and inverted images (right) showing severely malformed coccoliths withing large vesicles with cytoplasmic intrusions and 'ectopic' calcite production. Scale bars: (a) 2 mm, (b, c) 5 mm.

Figure S7. Diagram summarizing notable ultrastructure differences observed between HET and HOL *Calcidiscus leptoporus*. Drawings and corresponding SEM micrographs are approximately to scale with bars representing ~2 μm. Ch, chloroplast; CV, coccolith vesicle; Fl, flagella; G, Golgi body; Ht, haptonema; Mt., mitochondria; Nu, nucleus.

Table S1. Dimensions (in μm ± standard deviation) of mineralized and unmineralized scales in *Calcidiscus leptoporus*. *N* represents the number of scales analyzed per sample type.

Table S2. Statistical relationships between *Calcidiscus leptoporus* HOL and HET cells when grown in the presence of the SERCA-blocker thapsigargin. Both photosynthetic physiology (QY) and change in cell number (cells · mL^{-1}) are presented in this table. Both had an $n = 4$. *F*v/*F*m and change in cell number were statistically analyzed through a series of one-way ANOVAs. A Shapiro-Wilks test for normality was run and if the data passed a Brown-Forsythe and Holm-Sidak tests were performed to compare differences between the experimental groups and control samples. If the data were not normally distributed, then a Kruskal-Wallis and Dunn's test was performed to assess differences between groups. NS means not significant.

How to cite this article: Meyer, E. M., & Taylor, A. R. (2025). A comparison of calcification mechanisms in haploid and diploid cells of the coccolithophore *Calcidiscus leptoporus* (Murray & Blackman 1898). *Journal of Phycology*, *61*, 466–484. https://doi.org/10.1111/jpy.70006